Phase-averaged, frequency dependence of jet dynamics in a scaled up vocal fold model with full and incomplete closure

Nathaniel Wei,[1] Abigail Haworth,[1] Hunter Ringenberg,[1] Michael Krane,[2] and Timothy Wei[1,*]
[1]*Mechanical & Materials Engineering, University of Nebraska–Lincoln, Lincoln, Nebraska 68588, USA*
[2]*Applied Research Laboratory, Pennsylvania State University, State College, Pennsylvania 16802, USA*

(Received 4 May 2022; accepted 12 October 2022; published 20 December 2022)

This study focuses on frequency dependence effects on glottal jet dynamics with a focus on the physiological condition in which the vocal folds do not fully close. Incomplete closure occurs naturally in children and adult females. But there are also pathological conditions that can be problematic. Experiments were conducted using a 10× scaled-up model in a free surface water tunnel. Two-dimensional vocal fold models with semicircular medial surfaces were stepper motor driven inside a square duct with constant opening and closing speeds. Cases with complete vocal fold closure and incomplete closure to only 15% of the maximum gap were examined. Time-resolved digital particle image velocimetry and pressure measurements along the duct centerline were made at Re = 7200 over equivalent life frequencies from 52.5 to 97.5 Hz. Phase-averaged and cycle-to-cycle analysis of key contributors to sound production were conducted. As would be expected, acoustically relevant parameters, e.g., fluctuations in volume flow rate and transglottal pressure, are attenuated when vocal folds do not close completely. The key findings of this study, however, lie in statistical and dimensional scaling analysis of frequency dependencies of terms in the streamwise integral momentum equation. Specifically, the unsteady inertial term appears to become increasingly significant with increasing frequency and may be a key differentiator between lower frequency phonation, i.e., male voices, and the higher frequencies of children and adult females. These frequency effects, however, do not appear to be relevant to pathological conditions characterized by incomplete vocal fold closure.

DOI: 10.1103/PhysRevFluids.7.123102

I. INTRODUCTION

This study was motivated by differences in the dynamics of flow through vocal folds that do and do not fully close during phonation. While the canonical flow assumes full vocal fold closure during each oscillation cycle, there are physiological conditions, such as the presence of polyps or nodules, in which the folds never completely close. Examples of such conditions include vocal fold paralysis and paresis [1], Huntington's disease [2], and polyps [3], among others. From a pathological perspective, it is well known that when the folds do not close, sound generation is less efficient and the ensuing sound levels are lower than in normal phonation [4,5].

However, incomplete glottal closure also arises naturally, most often in children and adult females. It is also common in healthy children and adult women with the key distinction that there typically is not a loss of capacity or acoustic strength. Phonation of the vowel /i:/ was studied at three different loudness and pitch levels in a group of young adults, both male and female [6]. They found that incomplete glottal closure and the subjective measure of breathiness increased with loudness, particularly for the female subjects. In a follow-up study [7], glottal air flow and intraoral pressure

*Present address: Mechanical Engineering, Northwestern University, Evanston, Illinois 60208, USA.

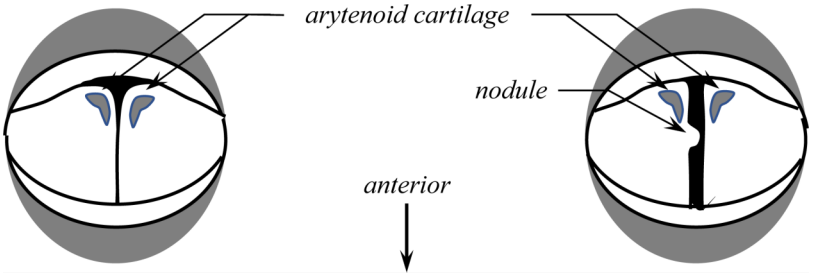

FIG. 1. Sketches of differences between incomplete vocal closure often found in healthy children and adult females (left) and due, for example, to polyps or nodules (right).

were measured coupled with video fiberstroboscopy and speech recordings to study phonation in a sample of healthy middle-aged women. It was shown that incomplete closure can be a natural result of aging in women. A more extensive study with a significantly larger number of adult subjects, and detailed, three-dimensional analysis of videostroboscopic data, was conducted [8] with generally consistent findings. High-speed digital video imaging was done [9] to expand this field of study to include children. Like the studies focused on adults, it was found that incomplete glottal closure was more prevalent in women, and that incomplete closure was also a common characteristic in prepubertal children, 5–11 years old.

It may be that the type and degree of incomplete closure is important. Often incomplete closure is characterized by a triangular opening at the posterior end of the folds near the arytenoid cartilage, while for pathological cases the opening is often along the entire glottal opening [10]. The qualitative difference between the two different types of incomplete closure is illustrated in Fig. 1. In both drawings, flow is out of the page with the speaker facing toward the bottom of the page. The sketch on the left shows the type of triangular shaped opening found in healthy children and adult females, while incomplete closure associated with pathological conditions is shown on the right. As can be seen, the opening caused by polyps or nodules can be more significant.

Incomplete closure, then, can be either pathological or simply a characteristic of morphology. The latter generally is not problematic, and, of interest relative to this study, it occurs in population groups that tend to have a higher fundamental frequency. This points to the need to better understand whether and how incomplete closure affects the dynamics of the glottal jet. At the core, there is a need to distinguish between frequency effects, i.e., adult males versus adult females and children, and noncanonical conditions such as incomplete closure. To this end, this paper builds on the work of Ringenberg *et al.* [11] to apply a measurements-based, integral momentum equation approach to better understand the role of different dynamics on the aeroacoustics associated with noncanonical vocal fold motions. The focus here is both on frequency effects on the canonical flow as well as effects due to incomplete closure.

A. Description of the canonical flow and key parameters

A sequence of vocal fold motions and associated flow across one canonical oscillation cycle is shown schematically in Fig. 2. Each drawing represents a different time step in the cycle. Flow is from bottom to top. The *glottis* is the gap between the vocal folds through which air flows. By convention, the upstream side of the vocal folds is referred to as *subglottal* and downstream of the folds is *supraglottal*. *Transglottal pressure*, then, refers to the pressure difference between the higher subglottal and lower supraglottal pressures. In the remainder of this paper, the orientation is rotated 90 ° to the right relative to Fig. 2, so the supraglottal region and flow direction is to the right. The flow is defined to be in the positive x-direction.

Figures 2(a) and 2(f) show the vocal folds at the beginning and end of the canonical cycle, respectively. When the cycle begins, pressure from the lungs opens the glottis by pushing the folds

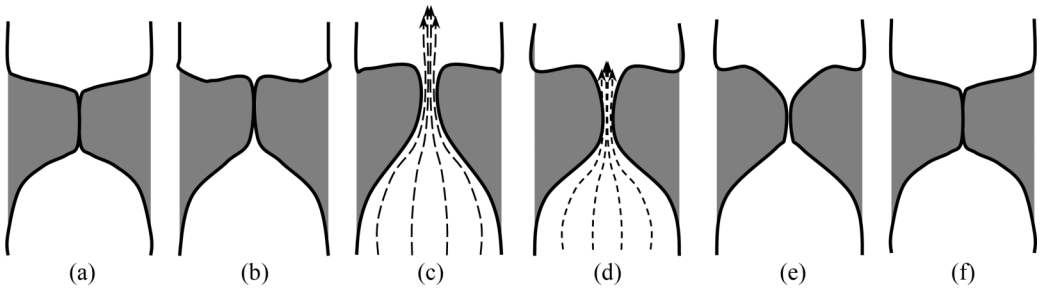

FIG. 2. Schematic of vocal fold motion showing opening (a)–(c) and closing (d)–(f) phases of one vocal fold vibration cycle. Dashed arrows denote airflow through the glottis when it is open.

upward, Fig. 2(b), and then outward, Fig. 2(c). Once opened, a jet, shown as dashed arrows, forms and the subglottal driving pressure decreases. As will be highlighted in Sec. I C, the glottal jet has been observed to turn to one side or the other, sometimes switching directions across cycles, and it also exhibits three-dimensional behavior as a function of geometry and frequency.

Later in the cycle, through combined aerodynamic pressure and elastic recoil effects, the vocal folds rock back and close, Figs. 2(d) and 2(e). The glottal jet pinches off and the folds return to their original position, Fig. 2(f). In human phonation, the vocal folds do not always close completely; this is the focus of the current paper. When they do close, however, they generally remain closed for 80–120 % of the time that the glottis is open, defined as T_o. In this work, the time open and the time the vocal folds are nominally closed are set to be equal so that the total oscillation period is $2T_o$. The time between Figs. 2(b) and 2(e), then, is approximately equal to the time between Fig. 2(f) back to 2(a).

The two characteristic nondimensional numbers used in this study are the Reynolds number, $\mathrm{Re} = U_{ss}\, h_{max}/\nu$, and reduced frequency, $f^* = fL/U_{ss}$, where h_{max} is the maximum glottal opening, U_{ss} is the steady-state bulk jet velocity when the vocal folds are held fully open, f is the oscillation frequency, and L is the vocal fold length in the streamwise direction. (In the literature, L, as defined here, is often referred to as the vocal fold "thickness.") Based on arguments presented by Krane *et al.* [12], vocal fold length is a more appropriate lengthscale for the jet dynamics than the glottal opening. There are two additional relevant frequencies referred to in this paper, namely f_{model} and f_{life}. The first, f_{model}, is the model vocal fold oscillation frequency, $1/2T_o$. This corresponds to an equivalent life frequency, f_{life}, that is 1500 times f_{model}. This factor stems from multiplying the ratio of kinematic air and water viscosities, $\nu_{air}\,\nu_{water} = 15$, by the square of the model to life scale (i.e., 10^2). Note that the velocity scale ratio, U_{life}/U_{model}, is then 150.

B. A brief literature review

There is an extensive body of work on flow associated with phonation. This includes a comprehensive literature review pertaining to the fluid mechanics of phonation [11,13]. Representative, more contemporary examples include work with excised fold models [14] and with *in vivo* models [15]. There are also studies using mechanical models [16,17].

A number of experimental studies [18–24] examined coherent structures, three dimensionalities, jet deflection, and switching in the context of sound production. There is a parallel body of computational studies [25–28]. While providing significant understanding and valuable insights, the focus of these works is heavily on kinematics and not dynamics. As such, the direct linkage between flow and acoustics is more observational than direct correlation to the underlying physics. The foundations and value of a dynamics-based (i.e., integral momentum equation) approach was developed by Ringenberg *et al.* [11].

In addition to the more canonical studies, there is a subbody of work specific to the problem of incomplete glottal closure [29–32]. One experimental study [29] combined single-point hot-wire anemometry and radiated pressure measurements to study the effects of posterior gaps on the glottal jet and sound generation. It was reported that incomplete closure resulted in increased turbulence and broadband noise. A combined numerical-experimental study of isotropic vocal fold models [30] was conducted to demonstrate the importance of body-layer stiffness in ensuring effective adduction. Using an excised canine model, it was shown that by increasing tension in the anterior-posterior direction, it could be possible to surgically correct certain physiological conditions. This is consistent with clinical findings [31] demonstrating that external vocal fold medialization using titanium implants was successful in addressing problems related to incomplete closure caused by vocal fold paralysis. A two-mass model with a triangular glottis [32] was developed to allow for delayed or incomplete closure not possible with conventional reduced order modeling.

In the computational domain [33], a model to produce speech associated with varying degrees of incomplete closure was developed. Untrained individuals were used to assess breathiness in the voice simulations and characterized breathiness in terms of vocal process separation and cepstral peak prominence. Computational methods [34,35] were also used to study flow and physiology related to incomplete closure and vocal hyperfunction. In the same manner as other experimental studies, they quantified the effects of incomplete closure using volume flow rate, pressure, and acoustic spectra. As with previous works on the canonical case, none of the studies on incomplete closure examined the problem from a dynamics perspective.

Irrespective of whether the research focused on canonical or noncanonical flows, the knowledge gap that the current and preceding work from this group addresses is understanding the acoustics of phonation from a dynamics perspective. The rationale here is that while aeroacoustic theory gives voiced sound in terms of vocal fold drag, the drag must be found from another relationship. Vocal fold drag appears explicitly in the streamwise integral momentum equation [11,35]. As such, understanding dynamics directly leads to a better understanding of the ensuing acoustics in ways that kinematics-based correlations cannot.

Demonstration of this approach and the first parametric study including flow and pressure measurements in a canonical scaled-up vocal fold model was done by Ringenberg *et al.* [11]. Using the same model as in this study, they examined phase-averaged and cycle-to-cycle variations over a range of Reynolds numbers, $3650 \leqslant \mathrm{Re} \leqslant 8100$, and reduced frequencies, $0.0141 \leqslant f^* \leqslant 0.0261$; the latter corresponded to an equivalent life frequency range of $52.5 \leqslant f_{\mathrm{life}} \leqslant 97.5$ Hz. In that study, the vocal folds started in a fully closed position, opened at constant speed for one quarter of an oscillation period, closed at the same speed for the second quarter of the period, and they remained closed for the final half-period. Data [11] directly validated the assertion [35] that the transglottal pressure force and vocal fold drag were quantitatively and qualitatively very similar over the entirety of a vocal fold oscillation cycle. It was also shown that, while small, the momentum flux and unsteady inertia terms were not negligible. Finally, it was shown [11,36] that even for nominally highly repeatable and symmetric vocal fold motions, cycle-to-cycle variations, characterized by variations in jet direction and strength, were an inherent feature of these flows. It was hypothesized that weak residual motions immediately downstream of the vocal folds served as the perturbations that would affect the subsequent jet.

C. Scaling of the acoustics and integral streamwise momentum equations

The theoretical underpinnings enabling study of the aeroacoustics of human phonation dates back as early as 1955 [37–42]. The fact that voiced sounds occur below roughly 4500 Hz so that sound propagates in the airway as planar waves was used [43] to greatly simplify the problem, solve the equation developed by Ffowcs-Williams and Hawking [38], and formally identify principal sources of phonatory sound generation. Figure 3 shows a schematic of the human upper airway, centered on the aeroacoustic source region in the larynx. The domain of the problem is $x_{\mathrm{in}} < x_1 < x_{\mathrm{out}}$. For an acoustic source at (y_1, y_2), the sound pressure, P', was measured by an observer at (x_1, x_2), and is

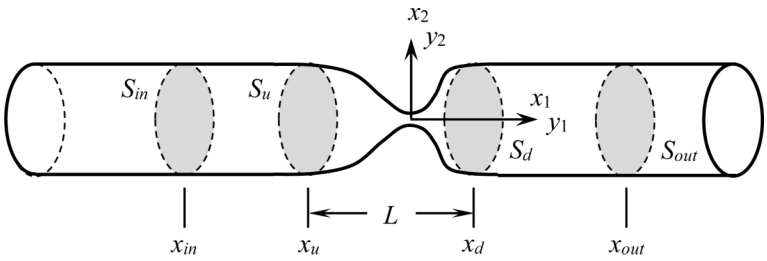

FIG. 3. Schematic drawing of the voice aeroacoustics problem. The domain of consideration is bounded by the control surfaces, S_{in} and S_{out} (i.e., $x_{\text{in}} < x_1 < x_{\text{out}}$), and the source region control volume, V_{larynx}, lies between x_u and x_d bounded by the surfaces, S_u and S_d. Coordinates for the observer and acoustic source are given by (x_1, x_2) and (y_1, y_2), respectively.

given by

$$p'(x_1, t) = -\frac{1}{2S}\iint_{S_{\text{VF}}}[\rho w_j n_j]dS_y - \frac{1}{2S}\iint_{S_{\text{VF}}}[p\,\text{sgn}(x_1 - y_1)]n_1 dS_y$$
$$- \frac{1}{2Sc}\frac{\partial}{\partial t}\iiint_{V_{\text{larynx}}}[\rho u_1^2]dV_y + \frac{1}{2S}\iint_{S_{in}}[\rho c u_1]dS_y - \frac{1}{2S}\iint_{S_{\text{out}}}[\rho c u_1]dS_y. \quad (1)$$

In this expression, u_1 is the fluid velocity, c is the speed of sound, w_j is the vocal fold wall velocity, p is the fluid pressure, n_j is the unit normal on the control surface, and the square brackets indicate evaluation at the retarded time $t - \frac{|x_i - y_i|}{c}$. The variables, S and V, denote surface areas and volume, respectively.

The first term on the right side of Eq. (1) is a volume source, i.e., a monopole, due to displacement by vocal fold wall motion. The second term is a dipole source due to vocal fold drag. The third term is a quadrupole due to direct radiation from glottal jet momentum fluctuations. The last two terms have been referred to as the action of additional sources [43]. For voiced sounds, however, they represent acoustic waves generated in the larynx that propagate out of the domain and reenter due to reflections. These reflections occur where the airway area changes, e.g., at the mouth or at the first bronchial branching in the lungs.

In phonation, the volume source term is thought to be weak at best because of the incompressibility of vocal fold tissues. Any volume fluctuations that might occur, therefore, would appear as a degenerate monopole that contributes to the sound field at the dipole level. Further, it has been demonstrated [35] that the ratio of the glottal jet quadrupole to the vocal fold drag is proportional to $\frac{f_0 L}{u_j}M$. This implies that the vocal fold drag dipole is the dominant source term at frequencies and Mach numbers typical of phonation.

In general, for a time-varying constriction in a duct that generates planar acoustic waves, the relative strength of the volume and drag sources may be different. These source strengths can be estimated directly from pressure and velocity field measurements. Specifically, the integral momentum conservation equation:

$$\rho\frac{\partial}{\partial t}\iiint_{V_{\text{larynx}}}u_1 dV + \rho\oiint_{S_{\text{larynx}}}u_1^2 dS = -\iint_{S_u+S_d}p\,dS + \oiint_{S_{\text{wall}}}\tau_{1j}n_j dS + F_{\text{drag}} \quad (2)$$

in the source region, i.e., $x_u \leqslant x \leqslant x_d$ in Fig. 3, provides information about the rate of change of source volume through measurement of the vocal fold wall motion. In addition, as can be seen in Eq. (2), the integral momentum equation also provides a means for a detailed understanding of the drag dipole source term using the same control volume. The integral momentum balance shows that vocal fold drag, F_{drag}, is the combined effect of, in order of appearance in Eq. (2), unsteady inertia, net momentum flux, the driving pressure force due to the transglottal pressure difference, and skin

friction drag. Finally, Eq. (1) states that the quadrupole term can be computed directly by integrating ρu_1^2 over the source volume.

In this study, the important connection between the acoustics equation, Eq. (1), and the streamwise momentum equation, Eq. (2), is the vocal fold drag. In the acoustics equation, vocal fold drag is the primary contributor to dipole source strength, while the momentum equation creates an avenue by which to quantify the vocal fold drag. Appropriate use of dimensional scaling analysis of both the momentum and acoustics equations, in turn, yields insights into the relative importance of terms as a function of frequency. For the momentum equation, all of the terms are nondimensionalized by the transglottal pressure, the first term on the right-hand side of Eq. (2). With respect to the acoustics equation, the issue of interest is the relative strengths of the monopole and dipole source terms, and whether the ratio of the two is frequency-dependent.

Beginning with the momentum equation, then, consider the unsteady inertia term, which can be scaled as

$$\rho \frac{\partial}{\partial t} \iiint_{V_{\text{larynx}}} u_1 dV \sim \frac{\rho u_j L S}{T_o/2}, \tag{3}$$

where u_j, L, and S are the glottal jet velocity, vocal fold length, and the cross-sectional area of the vocal fold duct, respectively. As will be seen later, for a two-dimensional duct, S is the glottal duct width, W, multiplied by a unit depth. Note that $T_o/2$ represents one-quarter of the oscillation cycle and is the time over which the vocal folds open and close; this is the appropriate timescale for the derivative. Next, the transglottal pressure force term may be scaled as

$$-\iint_{S_u+S_d} p \, dS \approx (P_u - P_d)S \sim \frac{1}{2}\rho u_j^2 \, S, \tag{4}$$

where P_u and P_d are the pressure on the upstream and downstream control surfaces located at x_u and x_d, respectively, as shown in Fig. 3. The ratio of unsteady inertia to the force due to the transglottal pressure difference is then

$$\frac{\rho \frac{\partial}{\partial t} \iiint_{V_{\text{larynx}}} u_1 dV}{(P_u - P_d)S} \approx \frac{\frac{\rho u_j L S}{T_o/2}}{\frac{1}{2}\rho u_j^2 \, S} = \frac{4L}{u_j T_o} = 8 f^*. \tag{5}$$

The key result of this analysis is that the importance of the unsteady inertia term scales with reduced frequency, f^*. According to Eq. (5), the inertia term will be of the same scale as the transglottal pressure force term around $f^* = 0.125$. The caveat, of course, is that the transglottal pressure force is always going to be greater than either the inertia or momentum flux terms, and if the inertia term actually becomes as large as the transglottal pressure force, the entire dynamics will be different. For the parameters as framed in this experiment, this corresponds to a life frequency, f_{life}, of ~467 Hz. While this is higher than the typical frequency range for children and adult women, it does indicate that unsteady inertia may be significant, i.e., of the same order of magnitude, in female and child phonation, or in soprano range singing (i.e., from ~260 to ~1050 Hz). That is, the assumption of the equivalence of the transglottal pressure force with vocal fold drag may not hold for higher frequencies. [As an aside, an argument could be made that $T_o/2$, the amount of time when the vocal folds are open and closed, may be too long given the rapid changes that occur when the vocal folds change direction. This would imply that the coefficient in Eq. (5) would be somewhat larger and that the unsteady inertia term would become significant at proportionally lower life frequencies. This only strengthens the conclusion that unsteady inertia effects may become significant within the normal ranges of child and female voices.]

For completeness, consider the ratio of the momentum flux term to transglottal pressure. The momentum flux term is dominated by the glottal jet acting across the gap opening. As such, the

momentum flux term in the streamwise integral momentum equation scales as

$$\oiint_{S_{\text{larynx}}} u_1^2 dS \approx \rho u_j^2 \, h_{\max}. \tag{6}$$

Note that this is expressed as momentum flux per unit depth. The ratio of momentum flux to transglottal pressure force is

$$\frac{\oiint_{S_{\text{larynx}}} u_1^2 dS}{\iint_{S_u+S_d} p \, dS} \approx \frac{\rho u_j^2 \, h_{\max}}{\frac{1}{2}\rho u_j^2 W} = 2\frac{h_{\max}}{W}. \tag{7}$$

Observe that the pressure force acts over the entirety of the glottal duct, S. For a two-dimensional geometry, S is the glottal duct width, W, multiplied by a unit depth. The key point of Eq. (7), then, is that both momentum flux and transglottal pressure force are to first order frequency-invariant, and their ratio scales as twice the ratio of the glottal jet width to the glottal duct width.

We turn now to the relative importance of the monopole source term in comparison to the dipole source strength (which is related to vocal fold drag). Recall that these are the first two terms on the right side of Eq. (1). Using similar dimensional arguments, the monopole term scales as

$$\frac{1}{2S} \oiint_{S_{\text{larynx}}} [\rho \, w_j n_j] dS_y \approx \frac{1}{2}\rho c \frac{h_{\max}}{T_o/2} L = \frac{\rho c h_{\max}}{T_o} L, \tag{8}$$

while the dipole term scales as

$$\frac{1}{2S} \iint p \, \text{sgn}(x_1 - y_1) n_1 dS_y \approx \rho u_j^2 W. \tag{9}$$

The ratio of the two terms, then, is

$$\frac{\frac{1}{2S}\iint_{S_{\text{VF}}} [\rho \, w_j n_j] dS_y}{\frac{1}{2S}\iint p \, \text{sgn}(x_1 - y_1) n_1 dS_y} \approx \frac{c h_{\max}}{u_j^2 \, T_o} \frac{L}{W} = \frac{1}{M_j} \frac{h_{\max}}{W} \frac{L}{u_j T_o} = \frac{1}{M_j} \frac{h_{\max}}{L} f^* \approx f^*. \tag{10}$$

To get to the final result in Eq. (10), observe first that $W \approx L$ and that the Mach number of the glottal jet is $O(10^{-1})$ as is the ratio, $h_{\max}/L$. The monopole source term would be equal in strength to the dipole term when $f^* = 1$. This corresponds to a life frequency, f_{life}, in excess of 3.7 kHz. Thus, in spite of its increasing importance with frequency, the monopole source strength is unlikely to be directly observed in general human phonation.

It is important to interject here that the current experimental model has a physiological limit in that, as pointed out in Sec. I, it is generally understood that the vocal folds deform in an incompressible manner. As such there actually is little to no change in the control volume due to their motions. In the present study, the in-and-out motion of the vocal folds does have a nonzero, albeit small, volume change. The most significant implication of this limitation is that the dimensional analysis result in Eq. (10) is likely too large; that is, the ratio of monopole to dipole source strength may actually be proportional to κf^*, where κ is a coefficient with a value much less than unity. In that case, the reduced frequency at which the monopole source strength would equal the dipole vocal fold drag would be much greater than 1, and the corresponding life frequency at which that would happen would be well outside the range of human phonation, i.e., it would only occur at frequencies greater than $3.7/\kappa$ kHz.

In terms of the relevance of the unsteady inertia term to the integral momentum balance, however, the effect of volume change with time is negligible in comparison to temporal variations of the glottal jet in the control volume. This was borne out by detailed analysis of the unsteady inertia term [11]. Those authors used scaling arguments as well as direct measurements to show that the increase in size of the control volume as the vocal folds open only admits a small additional amount of low momentum fluid, which contributes very little to the volume integral. In contrast, there is a significant increase in momentum as the glottal jet develops, transits across the control volume, and

then is pinched off when the vocal folds close. Thus, the contribution of the jet to the inertia term occurs irrespective of whether the control volume changes size. And the fact that Eq. (5) indicates a dependence on f^* on the ratio of unsteady inertia to transglottal pressure is therefore a basis for an argument that unsteady inertia can become significant in terms of phonation at higher reduced frequencies. This will be explored in detail in Sec. V C.

D. Problem statement

While the preceding scaling analysis provides valuable insights into how different terms in the governing equations might vary as a function of frequency, there remains an overarching question as to whether and how vocal fold drag and its surrogate, transglottal pressure, depend on frequency. This cannot be extracted from the analysis because transglottal pressure is the reference term against which the other terms are compared.

Further, these dimensional scalings do not account for the time-varying nature of the vocal fold cycle. That is, transglottal pressure and vocal fold drag have a roughly sinusoidal variation when the folds open and close while time traces of momentum flux simply increase and then decrease [11]. So, there are amplitude and phase relationships that also need to be explored.

The goal of this work, then, is to examine the frequency dependence of *all* terms in the streamwise momentum equation for the canonical case in a time-varying sense, and additionally to link the empirical and kinematic observations about the noncanonical case of incomplete vocal fold closure with the dynamics of glottal jets and the ensuing acoustics. Interesting questions, such as how incomplete closure affects the mass and momentum balance in the glottal jet, and how this affects aeroacoustic sources, can now be more directly addressed. With these motivations in mind, there are a number of specific fundamental questions addressed in this study. The first is whether or not there is a frequency dependence on transglottal pressure force and vocal fold drag, and if so, does that dependence change at different key points throughout the oscillation cycle? The second question is whether incomplete vocal fold closure affects glottal jet dynamics, and if so, is the transglottal pressure force still an effective surrogate for vocal fold drag? A third question is whether momentum flux and unsteady inertia is more or less important for incomplete closure. In addition, irrespective of whether the vocal folds close completely, is there a frequency threshold where transglottal pressure does not dominate the momentum balance? And finally, does the lack of vocal folds closure impact cycle-to-cycle variations?

II. APPARATUS

Temporally resolved pressure and flow-field measurements were made using a 10× scaled-up vocal fold model [11,12,44,45] in a large free-surface water tunnel [11]. A top-view installation schematic of the experimental apparatus is shown in Fig. 4. The glottal model consisted of a 28 cm × 28 cm × 366 cm (inside measure) duct with a square, closed cross-section into which two vocal fold models were inserted. The vocal fold models consisted of 12.7-cm-diam half-cylinders fixed to the ends of rectangular boxes such that the assembly was 14 cm wide × 12.7 cm in streamwise length × 28 cm high. Each was driven by a Servo System® stepper motor using a worm gear and linear stage. As shown in Fig. 4, each model was mounted onto two stainless-steel guideposts and fitted into an opening on either side of the glottal duct, 45.7 cm downstream of the duct entrance. It is assumed, particularly with phase averaging and an integral control volume spanning the entire glottal width, that the flow is nominally two-dimensional. As such, the dynamics and acoustics of this flow are dominated by the two-dimensional effects measured at the vocal fold midheight.

Ten 0.16-cm-diam pressure taps were drilled along the centerline of the duct ceiling. Defining the upstream and downstream faces of the vocal fold models as x_u and x_d, respectively, and the location of the glottis, i.e., the point of contact of the two opposing models, as x_g, the streamwise locations of the pressure taps were $(x - x_u)/(x_d - x_u) = -0.5, -0.25, 0, 0.25, 0.5, 0.75, 1.0, 1.25, 1.5$, and 2.0. Each tap was connected to a length of flexible tubing, which was, in turn, connected to a glass

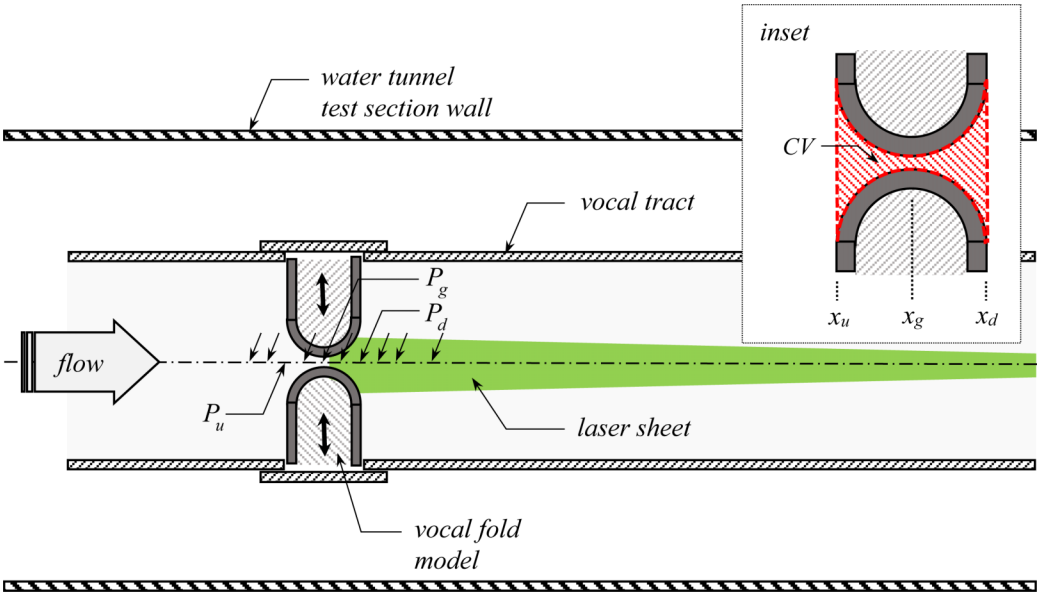

FIG. 4. Top-view installation drawing of scaled-up vocal fold model including stepper motor (not shown) driven vocal folds and vocal tract installed in a free surface water tunnel. Flow is left-to-right. A horizontal laser sheet is directed upstream with a camera (not shown) looking up from underneath the tunnel. Locations of 10 pressure taps are indicated with arrows; the upstream, P_u, glottal, P_g, and downstream, P_d, taps are indicated. The inset drawing shows the control volume in red and the upstream, glottal, and downstream locations, x_u, x_g, and x_d, respectively. Note that flow upstream of x_g was computed from continuity assuming uniform laminar flow.

tube manometer bank. The natural frequency of each manometer was conservatively estimated to be $\omega_n \approx 2.2$ rad/s [11]. This corresponds to a dimensionless time, $t/2T_o$, of ~0.03 for the highest frequency case in this study.

Experiments were conducted in a free-surface water tunnel [11] with a test section measuring 61 cm wide, 91.4 cm deep, and 500 cm long, and a maximum flow rate of approximately 10 000 lpm. The full glottal duct assembly was mounted on legs so that it was equidistant from the tunnel sidewalls and floor. The closed top of the duct was submerged to approximately 5 cm below the free surface.

Digital particle image velocimetry (DPIV) measurements were made using a Phantom Miro 310 high-speed video camera and a Quantel Evergreen EVG00200 dual pulse Nd:YAG laser. The laser had a maximum power of 200 mJ per pulse with a repetition rate of 15 Hz. Flow was seeded with 10 μm silver-coated glass spheres from Potter Industries. The camera, vocal fold stepper motors, and laser were synchronized by a Berkeley Nucleonics 565 Pulse Delay Generator.

Simultaneous video recordings of the time-varying manometer levels were made using a Raspberry Pi camera. The Raspberry Pi camera framed at 30 fps driven by its own onboard clock. The entire system, including vocal folds, laser, DPIV camera, and Raspberry Pi camera, however, was triggered by a common pulse from the pulse delay generator.

The two-dimensional (i.e., unit depth) integral control volume is shown in Fig. 4 as an inset and appears as the red shaded region. The upstream and downstream faces are colocated with the upstream and downstream faces of the vocal fold models and defined to extend across the entire width of the duct. Contributions to velocity integrals, such as the momentum flux term in Eq. (1), are identically zero everywhere along the flat parts of the vocal folds where there is no flow. The "lateral faces" of the control volume are defined to be the medial surfaces of the vocal fold walls.

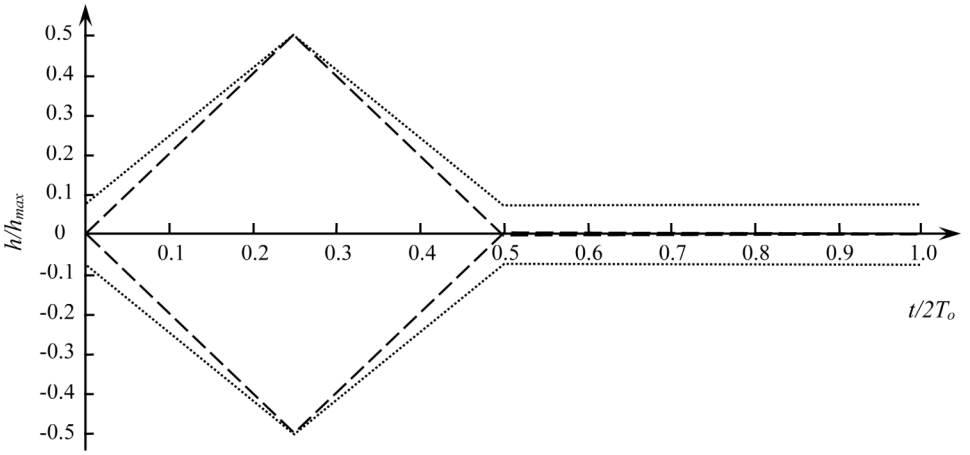

FIG. 5. Schematic time trace showing the two vocal fold motions in this study. The heavy dashed line indicates the canonical motion wherein the vocal folds fully close for half an oscillation period. The dotted line shows the motion where the vocal folds do not fully close. The ratio of incomplete closure to the full opening, $h/h_{\max}$, is 0.15.

III. METHODS

A. Experimental conditions

Following on the study detailed in Ref. [11], the goal of the present research was to examine the momentum balance in glottal jets where the vocal folds do not fully close, with an eye toward effects on sound production. This study focused on symmetric vocal fold motions over a range of Reynolds numbers and reduced frequencies characteristic of the adult human male voice.

Data sets for two types of vocal fold motion, shown schematically in Fig. 5, are presented in this paper. Both sets consist of measurements at a fixed Reynolds number and four different oscillation frequencies. The canonical baseline set involved vocal fold motions where the folds fully closed. The other set consisted of motions for which the folds only closed to 15% of the maximum gap, $h_{\max} = 22$ mm. As seen in Fig. 5, the vocal folds started from their nominally "closed" position, opened at constant speed to $h_{\max}$, closed at the same constant speed, and then remained at their nominally closed position for a time equal to the sum of the opening and closing times. It is recognized that in the physiologic condition where vocal folds do not close, the extended period of "closure" typically does not occur, i.e., the total oscillation period, T, is identically equal to the open time, T_o. Including the delay, however, was important in terms of direct comparison to the fully closed cases. Further, it is hypothesized that there is indeed physiological relevance to these experiments; this is addressed at the end of Sec. V B.

Vocal fold model frequencies, $f_{\text{model}} = 1/2T_o$, were 0.035, 0.045, 0.055, and 0.065 Hz. Adjusting for the 10× scale of the vocal fold models relative to physiological scale, and the fact that the kinematic viscosity of air is 15 times that of water, these frequencies correspond to life-scale frequencies, f_{life}, of 52.5, 67.5, 82.5, and 97.5 Hz, respectively. The Reynolds number, based on $h_{\max}$ and a steady-state jet speed, U_{ss}, of 31.6 cm/s, was 7200.

For every case studied, the tunnel speed was set with the vocal folds in their nominally closed position, i.e., $h = 0$ for the canonical cases and $h = 0.15h_{\max}$ for the partial closure cases, and allowed to run for a minimum of 30 min before vocal fold motions were initiated. This ensured that the bulk flow around the outside of the duct model was steady. It was argued in [45] and quantitatively verified [11] that the opening of the vocal folds had a negligible effect on the subglottal pressure. Further, it was shown [11] that the flow around the outside of the duct had no effect on the glottal jet dynamics.

To ensure adequate sample sizes for phase-averaging, a minimum of 20 oscillation periods were captured for each case. Thus, for the cases at 0.065 Hz, three sets of eight consecutive oscillations were captured. For the 0.035, 0.045, and 0.055 Hz cases, five sets of four, six sets of four, and three sets of seven consecutive oscillations were captured, respectively. In addition, pressure and velocity measurements were also made under steady-state conditions where the vocal folds were fixed in the fully open position. One thousand vector fields were captured for these steady-state fully open cases over a span of 67 s. Pressure measurements were made when the vocal folds were fully closed with the water tunnel pump running at the setting corresponding to Re = 7200. Since there was no flow through the vocal fold models, flow measurements were unnecessary.

B. DPIV measurements

Time-resolved flow-field measurements were made at the midheight of the glottal model. The camera field of view was 21.9 cm × 16.4 cm in the x- and y-directions, respectively, with a pixel resolution of 54.8 pixels/cm. The flow was illuminated with an ∼0.1-cm-thick sheet from a dual pulse Nd:YAG, as illustrated schematically in Fig. 3. DPIV image pairs were captured with the digital video camera below the water tunnel test section, positioned with flow from left to right and the glottis located just inside the left edge of the field of view. The capture rate for image pairs was 15 Hz for a minimum of 230 vector fields per oscillation cycle (at the highest frequency), and the time between images in a pair, δt, was 1.5 ms.

The stepper motors, DPIV camera, and laser were driven and synchronized by a common master clock on the pulse delay generator. DPIV vector fields were computed using a two-stage cross-correlation algorithm [46,47] with 128×128 pixel windows for coarse displacement fields followed by 32×32 pixel "fine" correlation windows. Four-times oversampling was used so that vectors were 8 pixels apart in both directions, corresponding to 0.146 cm in physical space. The uncertainties for maximum jet velocity, volume flow rate, and the unsteady inertia term in the streamwise integral momentum equation [11], presented in Sec. IV, are roughly 0.7% of their respective maximum values. Since momentum flux and dynamic pressure are proportional to streamwise velocity squared, the uncertainty of those measurements is ∼1.4% of their respective maxima. Of course, assuming the error is stochastic, phase-averaging and integration should reduce these uncertainties.

C. Pressure measurements

The locations of the 10 pressure taps were described in Sec. II. Water heights in the glass manometer bank were imaged and recorded using a Raspberry Pi camera at 30 fps at a resolution of 80 pixels/cm. The temporal resolution of the pressure measurements was better than 0.5 s and the manometer resolution was better than the meniscus height of 0.05 cm or 5 Pa. This is less than 6% of the maximum transglottal pressure values measured in this study. A frequency response analysis of the manometers [11] indicated that the maximum delay in the manometer response, corresponding to $t/2T_o \approx 0.03$, would occur for the fully closed cases when the vocal folds first opened, closed, and when they changed direction. This is sufficiently fast to resolve even the largest pressure fluctuations.

For each oscillation cycle in each run, the Raspberry Pi camera was triggered by a pulse from the master clock on the Berkeley Nucleonics pulse delay generator. DPIV and Raspberry Pi video capture rates for flow and pressure measurement, respectively, were synchronized to within ±1 ms over each vocal fold oscillation period. To quantify pressures, video images were converted to binary using a threshold level that clearly and sharply defined the menisci of each manometer column. The centroid of each meniscus along the manometer centerline was computed. This centroid location was used as the column height for each manometer in every video image.

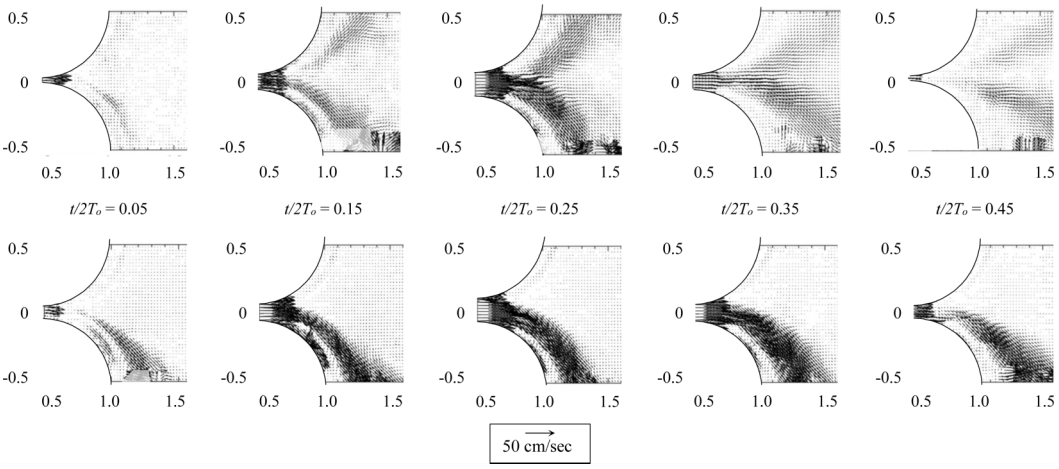

FIG. 6. Phase-averaged velocity fields for the canonical, fully closed case (top row) and incomplete closure case (bottom row) for six time steps when the vocal folds open and close. Both sets of velocity fields were for the highest-frequency case, $f_{\text{life}} = 97.5$ Hz. Nondimensional times are indicated between the two rows, and a reference vector for scale has been added. What appears to be a bifurcation of the jet in the fully closed case is an artifact of cycle-to-cycle variations.

IV. RESULTS

Simultaneous DPIV and pressure measurements were made in a scaled-up vocal fold model in a large free surface water tunnel. Four different frequencies at a Reynolds number of 7200 were studied for the conditions in which the vocal folds closed completely and only partially after each oscillation cycle. The model frequencies, f_{model}, were 0.035, 0.045, 0.055, and 0.065 Hz corresponding to life frequencies, f_{life}, of 52.5, 67.5, 82.5, and 97.5 Hz, respectively. Results from these experiments are presented in this section. To provide reference points, measurements of pressure and velocity were also made for the steady-state cases where the vocal folds were fixed in their fully open position and subsequently in the fully closed position at the four different Reynolds numbers; these are the "steady-state" cases. Finally, at the outset, it is noted that all of the fully closed case data, presented in Figs. 6–11, were first published by Ringenberg *et al.* [11].

A. Phase-averaged velocity measurements

Figure 6 shows two sequences of five phase-averaged DPIV vector fields at nondimensional times $0.05 \leqslant t/2T_o \leqslant 0.45$. This spans the time just after the vocal folds begin to open to just before they return to their initial position. Flow is left-to-right with the vocal folds masked in white. The top row is for the case in which the vocal folds fully close and the bottom row shows the flow when the folds do not close completely. Both cases were for $f_{\text{life}} = 97.5$ Hz. For clarity, only every other vector is shown. Observe that a small patch of spurious vectors appears at the very bottom of some of the vector fields, specifically the last four frames in the top row and the first frame in the bottom row. These are artifacts arising from spurious vectors in a single oscillation, and they lie outside of the control volume where any analysis was conducted; they have been partially masked to minimize the visual effect.

The salient feature of Fig. 6 is that the phase-averaged jet appears to be bifurcated in the top row for the case in which the vocal folds fully close, but it turns to the right (i.e., downward in the orientation shown) for the incomplete closure case in the bottom row. What appears to be a bifurcation is a manifestation of averaging over multiple cycles where there is significant cycle-to-cycle variation including jet switching. It was hypothesized [11] that this phenomenon was caused

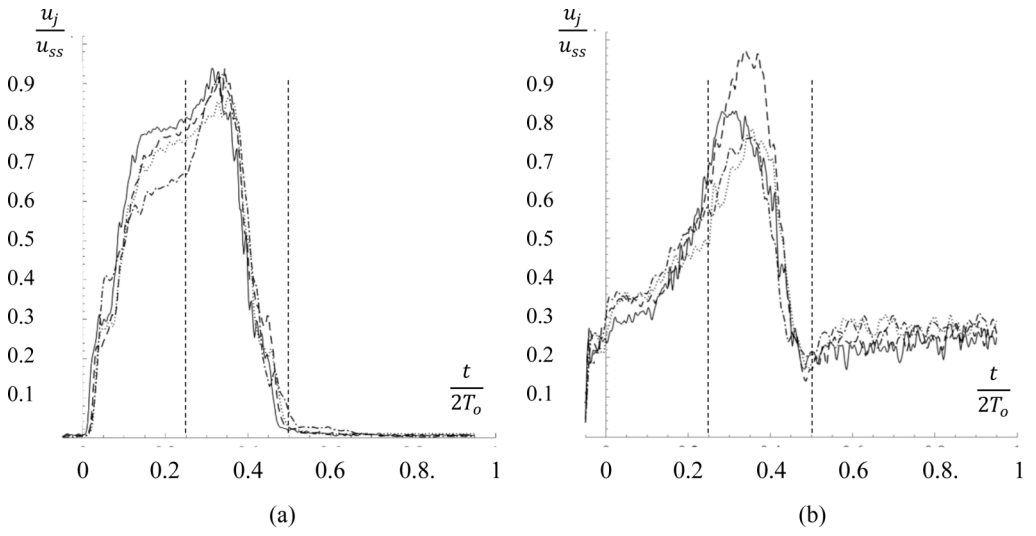

FIG. 7. Time traces of u_j/u_{ss} for all four oscillation frequencies at (a) for the fully closed case and (b) the incomplete closure case. Dotted vertical lines indicate the times, $t/2T_o = 0.25$ and 0.5, when the vocal folds are fully opened and when they return to their fully or incompletely closed positions.

by residual unsteady motions downstream of the vocal folds after they completely close. Thus, cycle-to-cycle variations in jet direction appear to occur far more frequently in the case of complete glottal closure than for incomplete closure.

Figure 7 shows phase-averaged time traces of maximum jet velocity, u_j, along the vocal-fold exit plane, x_d, for the four frequencies for the fully closed cases in Fig. 7(a) and the corresponding incomplete closure cases in Fig. 7(b). In these plots, u_j has been nondimensionalized by the averaged glottal jet bulk velocity, u_{ss}, measured in the fully open, steady-state condition corresponding to Re = 7200. For these traces and all subsequent ones, time is nondimensionalized by the oscillation period, $2T_o$, where $t/2T_o = 0$ and 0.5 correspond to when the vocal folds begin to open and when they return to their fully or incompletely closed positions. For this and subsequent figures, vertical dashed lines have been placed at $t/2T_o = 0.25$ and 0.5 to indicate when the vocal folds are fully open and nominally closed, respectively.

For the fully closed case, Fig. 7(a), there is a pressure build up across the vocal folds which is released when the folds begin to open. This feature, which will be further discussed in Sec. IV B, results in an impulsively started jet and a corresponding rapid increase in maximum jet velocity. By comparison, the transglottal pressure difference for the incomplete closure cases is not as large and, as seen in Fig. 6, a glottal jet persists throughout the cycle. As such, the glottal jets for the incomplete closure cases do not start impulsively and there is a more gradual increase in maximum jet velocity. This is readily seen in comparing corresponding time traces in Figs. 7(a) and 7(b).

Another difference is the clear frequency dependence for the fully closed cases, Fig. 7(a), which are not as distinct in the incomplete closure cases, Fig. 7(b). In Fig. 7(a), it can be seen that at any given time in the range $0.1 \lesssim t/2T_o \lesssim 0.3$, u_j/u_{ss} decrease with increasing frequency. The peak values, however, are the same and occur at the same time, $t/2T_o = 0.35$, for all four frequencies. No such clear trend is visible for the incomplete closure cases.

One can see in both plots comprising Fig. 7 that the jet actually continues to accelerate after the vocal folds begin to close. The jet velocity, therefore, does not peak until around $t/2T_o \approx 0.35$. This is attributed to the combined effect of a buildup in the transglottal pressure difference as the vocal

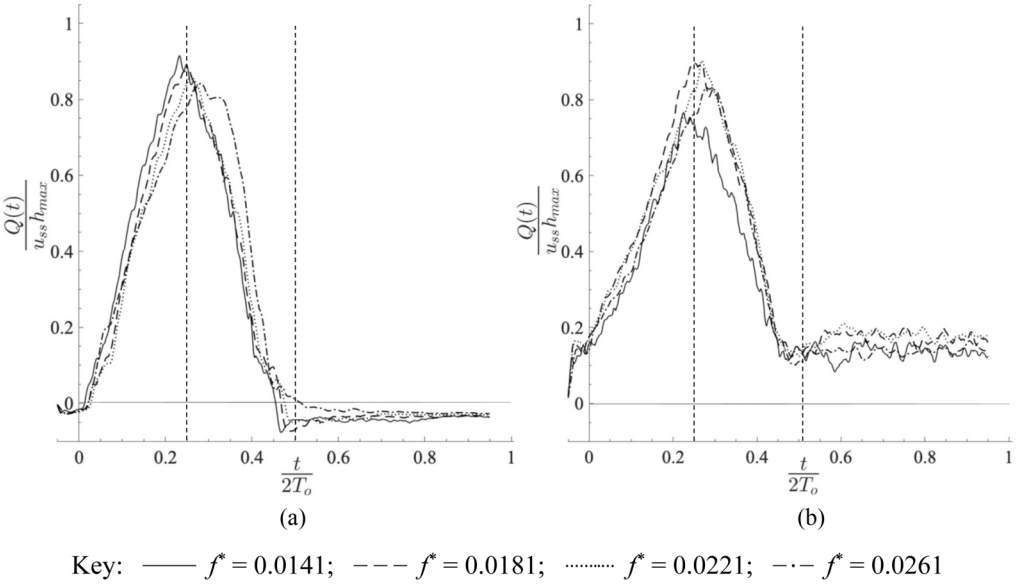

FIG. 8. Time traces of volume flow rate through the vocal fold exit plane for all four oscillation frequencies at (a) for the fully closed case and (b) the incomplete closure case. Dotted vertical lines indicate the times, $t/2T_o = 0.25$ and 0.5, when the vocal folds are fully opened and when they return to their fully or incompletely closed position.

folds begin to close and the inertia of the duct flow as it is forced to move through a decreasing opening. The contrast between the fully closed and incomplete closure cases is due, then, to the fact that the flow inertia changes by a greater amount for complete closure than it does for incomplete closure when the jet never shuts off. It is important to recognize that this effect is related to the reversal of the vocal fold motion at $t/2T_o = 0.25$. One would therefore expect to see continued acceleration in the range $0.25 \leqslant t/2T_o \lesssim 0.35$, irrespective of whether the vocal folds are fully closed at the start of the oscillation cycle.

Phase-averaged traces of volume flow rate (per unit depth) across the vocal fold exit plane are given in Fig. 8. The volume flow rate was computed by integrating the phase-averaged streamwise velocity across the vocal fold exit plane at each time step. Data were nondimensionalized by steady-state bulk velocity, U_{ss}, and maximum glottal opening, h_{max}. Time was scaled by $2T_o$. As with the preceding figure, Figs. 8(a) and 8(b) show the fully closed and incomplete closure cases, respectively.

For the fully closed cases, Fig. 8(a), the traces increasingly tilt to the right, and the maximum nondimensional flow rate decreases with increasing frequency. The tilt is a manifestation of vocal tract inertance and the jet being pinched off by the closing vocal folds, as discussed previously. When the cycle begins with no fluid motion, the change in flow inertia in the vocal tract is much larger than for the case of incomplete closure. As a result, the volume flow waveform tilt is more pronounced in the complete closure cases, and it shows a stronger trend with frequency. As discussed in Ref. [11], the small negative volume flows after closure seen in Fig. 8(a) are due to residual jet circulations across the vocal fold exit plane where the measurements were made.

The tilting and decrease in volume flow rate show similar trends for the incomplete closure cases shown in Fig. 8(b). They are, however, less pronounced. An exception occurs at the lowest frequency, $f^* = 0.0141$. For that case, the maximum volume flow rate is less than that for the higher three frequencies. In the fully closed cases, the maximum volume flow rate is largest for the lowest frequency.

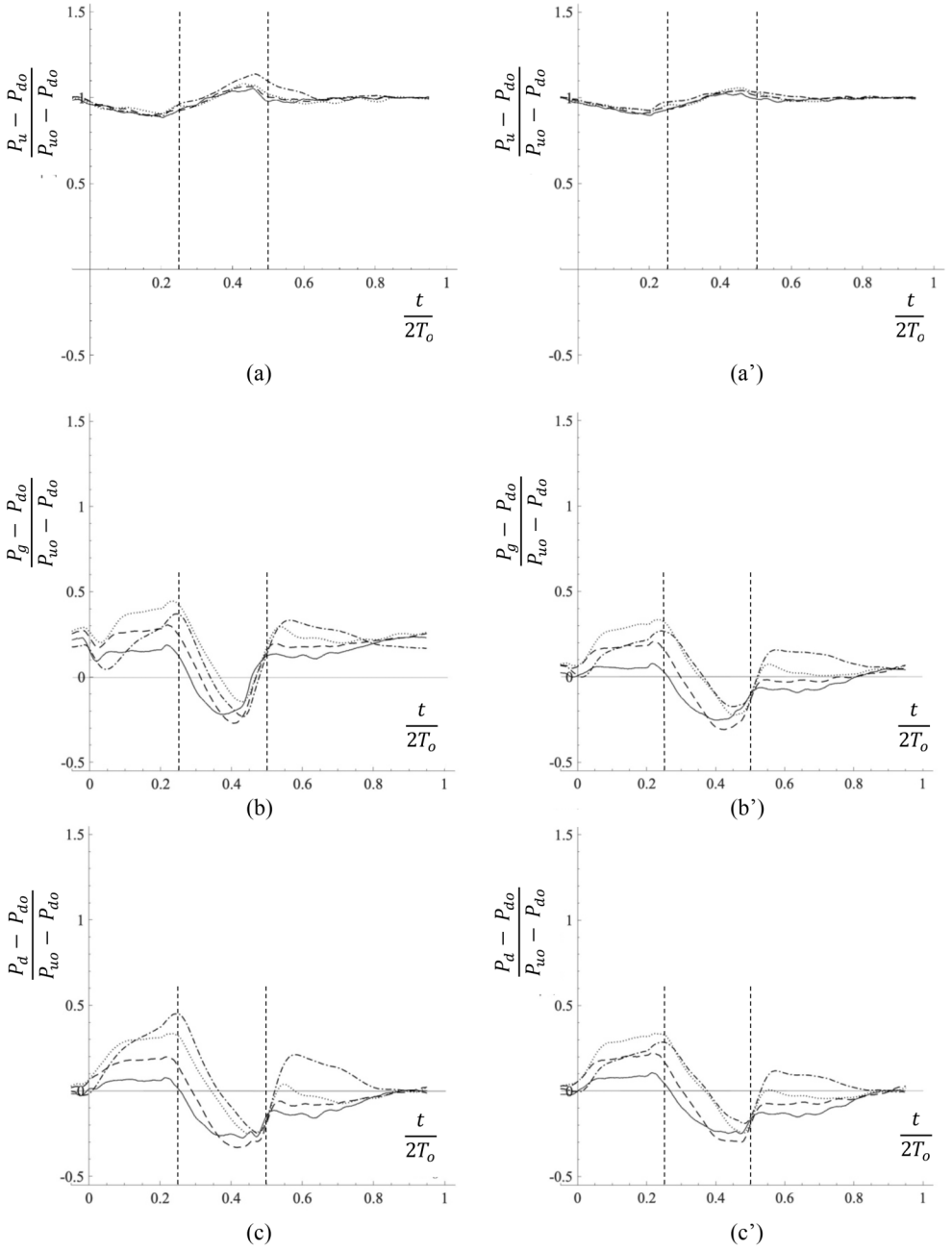

FIG. 9. Time traces of (a) upstream, (b) glottal, and (c) downstream pressure coefficients for the four oscillation frequencies with full vocal folds closure. Parts (a′), (b′), and (c′) are the corresponding incomplete closure cases. Dotted vertical lines at $t/2T_o = 0.25$ and 0.5 indicate when the vocal folds are fully opened and when they return to their nominally closed position.

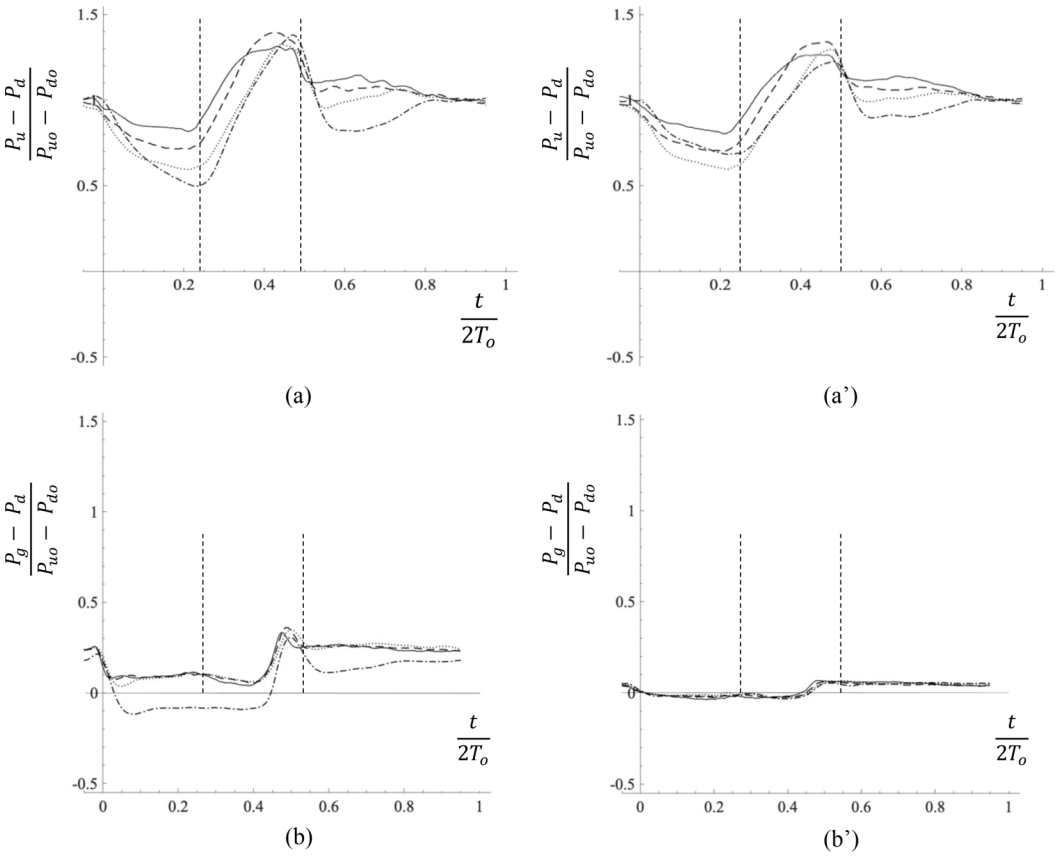

FIG. 10. Phase-averaged transglottal pressure time traces for the four oscillation frequencies with full vocal fold closure (a) and incomplete closure (a′). The corresponding nondimensional supraglottal pressure differences are shown in (b) and (b′), respectively.

For completeness, it should be pointed out that the jet velocity in the incomplete closure trace for the second lowest frequency, $f^* = 0.0181$, in Fig. 7(b) appears to have a higher maximum than the three other frequencies. To a lesser degree, this can also be seen in the phase-averaged traces shown in Fig. 8(b). The reason for this is not clear at this point. This higher flow is consistent with the corresponding transglottal pressure trace in Fig. 10(a′), which is presented in the following section. Given that the DPIV and pressure measurements were simultaneous but completely independent, it is unlikely that the traces were the result of measurement or processing errors. Further, they do not affect the broader analysis and conclusions in this study.

B. Phase-averaged pressure traces

Time traces of phase-averaged pressure coefficients are shown for the four different frequencies with full and incomplete closure in Fig. 9. The phase-averaged pressure at the upstream face of the vocal fold model, P_u, Figs. 9(a) and 9(a′), at the glottis, P_g, Figs. 9(b) and 9(b′), and at the exit plane, P_d, Figs. 9(c) and 9(c′), are referenced to the mean downstream exit pressure when the vocal folds are closed, P_{do}, and normalized by the mean transglottal pressure difference when the folds are

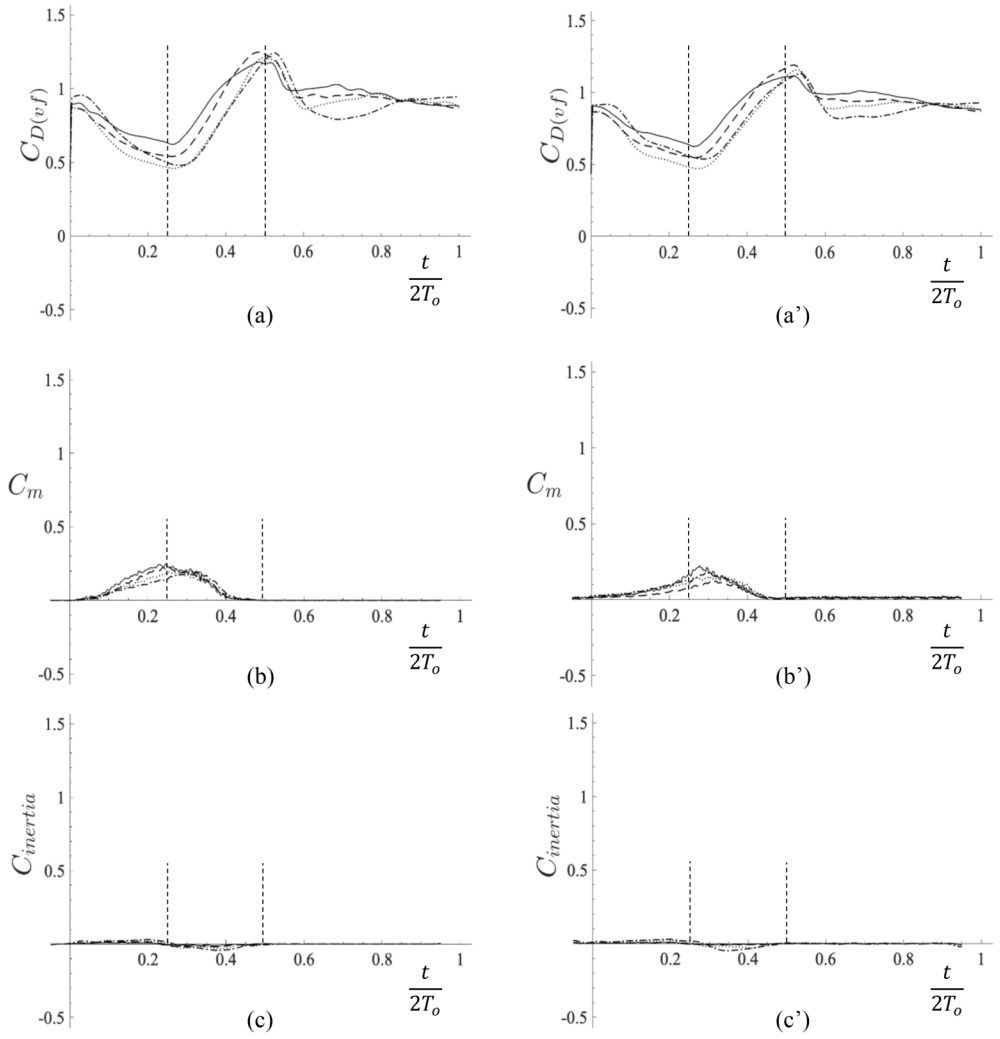

FIG. 11. Time traces of phase-averaged terms in the streamwise integral momentum equation for the four oscillation frequencies: (a) vocal fold drag, (b) streamwise momentum flux, and (c) inertia. Plots for the fully closed cases appear on the left. Data for the incomplete closure cases appear on the right with primes, (a′), (b′), and (c′), respectively.

closed, $P_{uo} - P_{do}$. For these and subsequent pressure plots, P_{uo} and P_{do} were the time-averaged values of the phase-averaged pressure signals at the upstream face, P_u, and the downstream face, P_d, over the time interval $0.85 \leqslant t/2T_o \leqslant 0.95$. This interval was chosen to best represent the supraglottal and subglottal pressures when the vocal folds were in their nominally closed positions; it was shown [11] that even after a time T_o, the supraglottal pressure P_d does not relax back to the steady state value $P_{d\text{-closed}}$. It was argued that this was due to the combined effects of the time the glottal jet needed to traverse the entire length of the supraglottal duct and the time required for any residual circulations set up by the jet to decay. Time is again nondimensionalized by the full oscillation period, $2T_o$.

Before examining the phase-averaged pressure traces in detail, it should be noted that the waveforms in Fig. 9 follow the principal trends of the waveforms measured directly in a live human larynx [48], in excised canine larynges [49], in a simulated self-oscillating glottis [50], as well as in driven models [51,52]. The agreement between this variety of experiments and the current study supports the assertion that the current reduced order physical model captures the essential features of glottal jet dynamics.

Returning to Fig. 9, then, while there are clear differences in the downstream pressure traces, Figs. 9(c) and 9(c′), there are noteworthy differences for the upstream and glottal pressure traces as well. It can be seen in Fig. 9(a) that as the vocal folds open, the upstream pressure decreases by about 10%. Just before the folds reach their maximum open position and begin to close, $t/2T_o \approx 0.25$, the subglottal pressure begins to increase and overshoots by around 10% when the folds close. The decrease is due to the release of pressure as the folds open, while the increase is a result of restricting flow on the upstream, or subglottal, side when the folds start to close. Shortly after closure, P_u quickly settles back to P_{uo}, though for the highest frequency, the return to P_{uo} takes a comparatively longer nondimensional time.

Very similar variations are visible for the subglottal pressure in the incomplete closure cases, Fig. 9(a′). However, where the maximum value of the subglottal pressure for the fully closed case at the highest frequency, $f^* = 0.0261$, is approximately 1.15, it is about 1.05 for the same frequency in the incomplete closure case. Note that for all other cases, the maximum dimensionless subglottal pressure values are all close to 1.05. It can also be seen that the ramp down from that maximum value is more gradual for the incomplete closure cases.

Similar trends can be observed for the minimum supraglottal pressure occurring in the range $0.35 \lesssim t/2T_o \lesssim 0.45$. These are presented in Figs. 9(c) and 9(c′). For the highest frequency, the minimum supraglottal pressure is –0.25 for the fully closed case, while it is –0.20 for the incompletely closed case. Finally, observe that there is a pressure overshoot for this highest frequency at $t/2T_o \approx 0.57$ just after the vocal folds reach their nominal closed positions. The dimensionless pressure values are 0.2 and 0.1 for the full and incomplete closure cases, respectively. There is a small pressure overshoot for the full closure case at $f^* = 0.0221$, the second highest frequency, but none of the other cases exhibit such an overshoot.

C. Phase-averaged dynamics; terms in the streamwise integral momentum equation

Key terms in the integral streamwise momentum equation are shown in Figs. 10 and 11. For comparison, they have all been nondimensionalized by $(P_{uo} - P_{do})S_{\text{duct}}$, where S_{duct} is the cross-sectional area of the duct. Starting with the right-hand side of Eq. (1), the driving pressure force is the transglottal pressure multiplied by the cross-sectional area of the glottal duct. Nondimensionalization, then, identically results in the transglottal pressure coefficient shown in Figs. 10(a) and 10(a′) for the fully closed and incomplete closure cases, respectively. Since the subglottal pressure, P_u, does not vary greatly across the oscillation cycle, cf. Figs. 9(a) and 9(a′), phase-averaged traces of transglottal pressure coefficient are qualitatively similar to the downstream pressure traces in Figs. 9(c) and 9(c′). As with P_d, the amplitudes of the nondimensional phase-averaged traces of $(P_u - P_d)$ are attenuated for the incomplete closure cases in comparison to their fully closed counterparts. The strong frequency dependence seen in the fully closed cases is again present, but less evident, in the incomplete closure cases.

Though not directly a part of the streamwise integral momentum equation, dimensionless traces of downstream or supraglottal pressure difference, $(P_g – P_d)$, are also included in Fig. 10. The fully closed and incomplete closure cases are shown in Figs. 10(b) and 10(b′), respectively. From a broad perspective, both figures show that the region between the glottis, x_g, and the downstream exit plane of the vocal folds, x_d, where the jet is located, makes a small, though measurable, contribution to the transglottal pressure difference in the case of full closure, but almost no contribution in the incomplete closure case.

There are some interesting features to these traces, however. For the fully closed cases, the highest-frequency case does not coincide with the three lower frequencies. It is hypothesized that this may be due to a small shift in the separation point for the jet at the higher f^*. The incomplete closure cases, in comparison, show even less variation. This is likely due to the fact that there is always a glottal jet and the gradients are therefore not as strong when the vocal folds first open and when they reach their nominally closed positions.

The closest comparison for these measurements is that of Deverge *et al.* [52]. In their study, they used rounded vocal folds similar to those in this study. However, they only moved one of the folds, while the other, fitted with a pressure transducer, was stationary. More importantly, their experiments were in air and their model vented directly to atmosphere; there was no vocal tract downstream of their vocal fold models. Further, their downstream pressure was the reference atmospheric pressure. With those differences in mind, their study also showed that there is an attenuation of the supraglottal pressure difference across the entire oscillation cycle.

Time traces of vocal fold drag, net streamwise momentum flux, and unsteady inertia terms for the full and incomplete closure cases are shown in Figs. 11(a)–11(c), respectively. Following conventions, the fully closed cases are on the left, and their incomplete closure counterparts are on the right. As described in Ref. [11], vocal fold drag was estimated using the pressure measurements at the upstream and downstream faces of the vocal fold models as well as the two intermediate stations located at $(x-x_u)/(x_d-x_u) = 0.25$ and 0.75. The drag was computed as the difference of the upstream and downstream pressures multiplied by the area of the flat part of the model protruding into the duct, plus the difference of the pressures at the intermediate stations multiplied by the radius of the cylindrical section times the duct height. Force coefficients were defined using transglottal pressure when the vocal folds were closed, $P_{uo}-P_{do}$, and S_{duct}. Finally, contributions to the momentum flux and inertia terms downstream of the glottis were computed directly from the DPIV velocity measurements. Flow upstream of the glottis was computed from continuity assuming uniform laminar flow at every streamwise location as described by Ringenberg *et al.* [11].

Comparisons between Figs. 10(a) and 11(a) and between Figs. 10(a′) and 11(a′) reveal that there is both qualitative as well as quantitative similarity between the driving pressure force and vocal fold drag. This was discussed at length [11] as evidence that transglottal pressure is an accurate surrogate for vocal fold drag, which, in turn, is a direct measure of acoustic source strength [35]. In terms of comparing between full and incomplete closure, i.e., between Figs. 11(a) and 11(a′), the same observations made for Figs. 10(a) and 10(a′) of attenuated peaks for the incomplete closure cases are relevant here as well.

The changing relative importance of the net streamwise momentum flux and the unsteady inertia term with increasing f^* are readily apparent in Figs. 11(b) and 11(b′) and Figs. 11(c) and 11(c′), respectively. One can see that momentum flux is small but not negligible. Note that the contribution from the upstream face of the control volume is not included, but this was shown using dimensional arguments to be an order of magnitude smaller than the momentum flux of the jet crossing the downstream exit plane [11].

The maximum values for time traces of the inertia term are even smaller than those of the momentum flux term. However, the maximum values of C_{inertia} increase with increasing f^* and occur just before the vocal folds close. The importance of the inertia term at higher reduced frequencies will be explored in greater detail in Sec. V C. For both the momentum flux and inertia terms, the amplitudes of variations are smaller for the incomplete closure cases relative to the full closure cases. The final term in the momentum balance is viscous shear. This was demonstrated [11,36] to be negligibly small.

V. DISCUSSION

It is widely understood that pathologies associated with incomplete vocal fold closure are accompanied by reduced fluctuations in transglottal pressure and volume flow rate [53–56]. These result in reduced sound levels and increased effort required to speak. Incomplete closure is also

observed in the context of gender and age, i.e., children and adult females versus adult males, though the physiology and geometry of incomplete closure is often different.

A cursory look at the results presented in the preceding section clearly shows frequency dependences as well as differences between full and incomplete closure. The frequency effects, however, appear to be similar regardless of whether the vocal folds fully close. As such, it seems plausible to examine frequency and closure as two somewhat independent effects. This discussion is therefore divided into three subsections. The first, Sec. V A, explores phase-averaged differences between full and incomplete closure. This provides insight into glottal jet dynamics irrespective of the reasons for incomplete closure. In the second subsection, Sec. V B, the topic of cycle-to-cycle variations is discussed as a function of whether the vocal folds close. The fully closed case was examined in detail in the preceding paper [11]. The final subsection, Sec. V C, builds from the scaling analysis developed in Sec. I C to develop insight into how jet dynamics may evolve with increasing frequency. This shows the power of the integral control volume approach and sheds light on how glottal aerodynamics is likely different for children and females in comparison with adult males.

A. Phase-averaged influences of incomplete closure on phonation

At the most basic level, the present experimental application of integral control volume analysis permits a more detailed, dynamics-based comparison of vocal fold oscillations that are fully closed versus those with incomplete closure. Differences in flow and pressure between these two cases were identified throughout Sec. IV. The most obvious and expected difference is that there is continuous flow past the vocal folds in the incomplete closure cases, while the flow is blocked for the fully closed cases.

Key differences emerge from the present measurement. First, for the fully closed case, the maximum jet velocity, u_j/U_{ss}, increases rapidly to a plateau, between 0.6 and 0.8 as a function of frequency, immediately after the folds begin to open. The plateau in the incomplete closure cases is much lower, rising only to approximately $u_j/U_{ss} = 0.3$. Second, for the fully closed case, there is a distinct increase in jet speed after the vocal folds reach their fully open position and begin to close, i.e., for $t/2T_o \geqslant 0.25$, which is attributed to the inertia of the jet encountering a decreasing opening. The phenomenon of rapid acceleration, plateau, and another rapid acceleration is not observed in the incomplete closure cases. Third, the maximum volume flow rates for the incomplete closure cases are lower than for their fully closed counterparts, particularly for the lowest frequency, $f^* = 0.0141$. This is in addition to the fact that the flow rate goes to zero for the fully closed cases but is nonzero for incomplete closure. Fourth, transglottal pressure waveforms for fully closed and incomplete closure cases look similar, but the fluctuation amplitudes are smaller for incomplete closure. And fifth, the transglottal pressure force is qualitatively and quantitatively similar to vocal fold drag for both incomplete and full closure. As with transglottal pressure, there is an attenuation in amplitude of fluctuations in the phase-averaged time traces of vocal fold drag for the incomplete closure cases.

There are two additional points here that warrant further exploration. The first is the maximum-to-minimum differentials of the phase-averaged volume flow rate traces in Fig. 8. As noted in the preceding paragraph, there is a degree of reduction in the maximum flow rate when comparing the incomplete closure cases with their fully closed counterparts. However, while there is no flow when the vocal folds are fully closed, the nondimensional flow rate for the incomplete closure cases is approximately 15% of the steady-state flow rate when the vocal folds are left open at their maximum gap, h_{max}; this is consistent with the fact that for these experiments, the minimum opening, h_{min}, was 15% of h_{max}. As a result, there is roughly a 20% reduction in the maximum-to-minimum differential in volume flow rate for incomplete closure relative to full closure. In terms of acoustics, it is this differential that is proportional to acoustic source strength. This approach, therefore, leads to a direct quantitative measure of the effects of incomplete vocal fold closure on phonation.

Second, there are differences in the downstream pressure difference, P_g–P_d, which may be quite important. These are seen in Figs. 10(b) and 10(b′) for the fully closed and incomplete closure cases, respectively. Observe that in Fig. 10(b), there are peaks in the time traces when the vocal folds first

open and when they close for the fully closed cases. These peaks are not present in the incomplete closure cases, Fig. 10(b′). In fact, for the incomplete closure cases, all four frequency traces overlap, and the maximum pressure difference is smaller than the subglottal pressure variations shown in Fig. 9(a′).

This implies that the glottal jet has little to no influence on transglottal pressure and, by extension, on vocal fold drag for the incomplete closure cases. This assertion is based on two observations. First, the downstream pressure difference is essentially zero from the glottis onward; for the incomplete closure cases, then, the transglottal pressure difference, P_u–P_d, and the upstream pressure difference, $P_u - P_g$, must be virtually identical. This holds at least over the range of reduced frequencies in this study. And second, the jet separation points in the phase-averaged velocity fields (not shown) do not vary with time, which further supports the notion that jet dynamics do not affect the downstream pressure.

In contrast, the jet formation in the fully closed cases is less predictable. An important implication of this is that the separation point moves both within a given oscillation and from one oscillation to the next, if for no other reason than the jet direction can switch from cycle-to-cycle. These variations will be discussed in the following section. As such, the dynamics of the forming glottal jet with each oscillation cycle influences the downstream pressure difference. As discussed in Ref. [11], greater spatial resolution of the pressure measurements in the glottal region would be required to address this issue in more detail. Neither the tap location for the glottal pressure measurement nor the DPIV vector spacing permit accurate determination of the jet separation point. It is hypothesized, however, that a moving separation point is the reason for the observed offset in the phase-averaged downstream pressure trace for the highest-frequency, fully closed case in Fig. 10(b). The key takeaway here, however, is that the lack of, or reduced, influence of the glottal jet on the transglottal pressure force, in the case of incomplete closure, effectively removes unsteady glottal jet dynamics from sound production, in comparison to the fully close cases.

In closing this section, some comments on the value and meaning of the phased-averaged analysis are appropriate. As is seen both here and in Ref. [11], this nominally canonical flow is quite complex, with multiple parameters and variations from cycle to cycle that appear to depend on some, if not all, of the parameters. The geometry and dynamics of the actual human vocal folds is even more complex; the current approach and study provide a structured pathway for unraveling all of the coupled interactions comprising the flow.

Given the complexity and variability of the flow, the approach taken here is analogous to decomposing a turbulent flow into mean and fluctuating parts. Phase-averaging here represents the mean, and the cycle-to-cycle analysis discussed in the following section is the counterpart of studying coherent structures in turbulence. Recognizing that phase averaging by itself does not provide a complete picture of the dynamics, it does, however, provide a framework with which to focus more closely on frequency dependence. It is, of course, the combination of the two approaches, namely phase-averaged and cycle-to-cycle variations, that provides the best picture of the flow.

B. Implications regarding cycle-to-cycle variations

Extensive reviews of phenomena associated with cycle-to-cycle variations were provided by Mittal *et al.* [13] and Ringenberg *et al.* [11]. Key features include side-to-side switching of the glottal jet with successive oscillation cycles, as well as variations in jet strength and corresponding amplitudes of the pressure fluctuations. Sherman *et al.* [36] observed a possible correlation between jet direction and jet strength; in their experiments, jets that deflected in one direction seemed to be consistently stronger than jets that deflected in the other direction. They also hypothesized that there may be a frequency dependence on jet switching, as over the frequency range of their study, cycle-to-cycle variations appeared to be more prevalent at some frequencies than others. Regardless of the universality of those particular observations, cycle-to-cycle variations appear to be characteristic of glottal jet flows, and they have been reported over a wide variety of physical experiments. They have been observed even in nominally highly symmetric geometries.

Detailed examination [11] led to the hypothesis that cycle-to-cycle variations arise from residual currents in the near supraglottal region while the vocal folds are closed. Flow in the supraglottal region was examined [11] for the fully closed oscillation case at the beginning of a run just before the vocal folds opened for the first time and at the very end of the first oscillation cycle, at $t/2T_o = 0.95$, after the vocal folds had been closed for almost half of the full oscillation period. It was observed that there was virtually no flow in the supraglottal region prior to the first vocal fold oscillation cycle, but that there was a weak counterclockwise current visible after that oscillation. Further, the glottal jet emerged straight out along the duct centerline for the first oscillation but was deflected to the right in the next oscillation. This was consistent with the direction of the weak current observed in the supraglottal region after the first oscillation. It was therefore hypothesized that these residual jet motions play an important role in setting the initial conditions. This idea was also discussed in the computational study of Zheng *et al.* [25]. The key difference was that the time their vocal folds remained closed was 80% shorter than in the present study, and the residual currents clearly did not have enough time to attenuate. Whether or not these currents are purely random or whether there is some functional dependence, e.g., on frequency or Reynolds number [36], is still an open question.

It is important to note that there is always a coherent glottal jet in the incomplete closure case. This is the dominant feature in the supraglottal region even when the vocal folds are closest together. Therefore, according to the hypothesis of residual currents, it is unlikely that cycle-to-cycle variations occur for incomplete closure. That this is the case was pointed out in Fig. 6, which compared vector fields of phase-averaged oscillation cycles for fully closed and incomplete closure cases. In the fully closed case, the phase-averaged glottal jet appears to be bifurcated. This is an artifact of the jet switching. Since the jet direction is different for different individual oscillations, the phase-averaged vector fields appear to show a bifurcated jet. In comparison, it was pointed out that the phase-averaged jet is not bifurcated in the incomplete closure case. It can be seen in Fig. 6 that the jet deflects downward for the orientation shown, indicating that the glottal jet deflected in the same direction for every individual oscillation cycle comprising the phase-averaged ensemble.

The lack, or at least the dramatic attenuation, of cycle-to-cycle variations is very significant in terms of phonation. As was also shown in Ref. [11], there is approximately 20% modulation in volume flow rate and 30% modulation in peak-to-peak transglottal pressure across just a few oscillation cycles for $f^* = 0.0261$ (corresponding to $f_{\text{life}} = 97.5$ Hz). These modulations are not present when the vocal folds do not completely close. Thus, while it is beyond the quantitative scope of this analysis, it is argued that this lack of modulations will strongly affect voice characteristics as the transglottal pressure force is directly related to the dominant acoustic source term; cf. Sec. I C. These effects, in turn, are different from those identified in Sec. V A.

A key consequence of the repeatability of the glottal jets for the incomplete closure cases ties back to the physiology of incomplete closure. Specifically, the approximately half-period delay, $1/2T_o$, that occurs during normal phonation is typically not present when the vocal folds do not completely close. In the incomplete closure cases, the vocal folds begin to reopen almost immediately after they reach their point of minimum closure. While the incomplete closure data presented here are valuable in terms of comparison to the fully closed cases, one could question whether or not they are physiologically relevant.

It is argued here that the answer to that question is "yes." This is because, unlike for the fully closed cases, there does not appear to be anything dynamically important that occurs during the half-period when the vocal folds remain in their minimum gap opening position. Evidence for that is the lack of any cycle-to-cycle variation, or alternatively, the high degree of repeatability for each successive oscillation. Where recirculation affects the direction and strength of the subsequent jet when the vocal folds close completely, the continuous glottal jet prevents the formation of those recirculation regions in the incomplete closure cases. As a result, it is argued that the jet dynamics for incomplete closure would be very similar, if not identical, whether or not there was a delay. And as such, it is hypothesized that the incomplete closure data may indeed be physiologically relevant even with the delay added in.

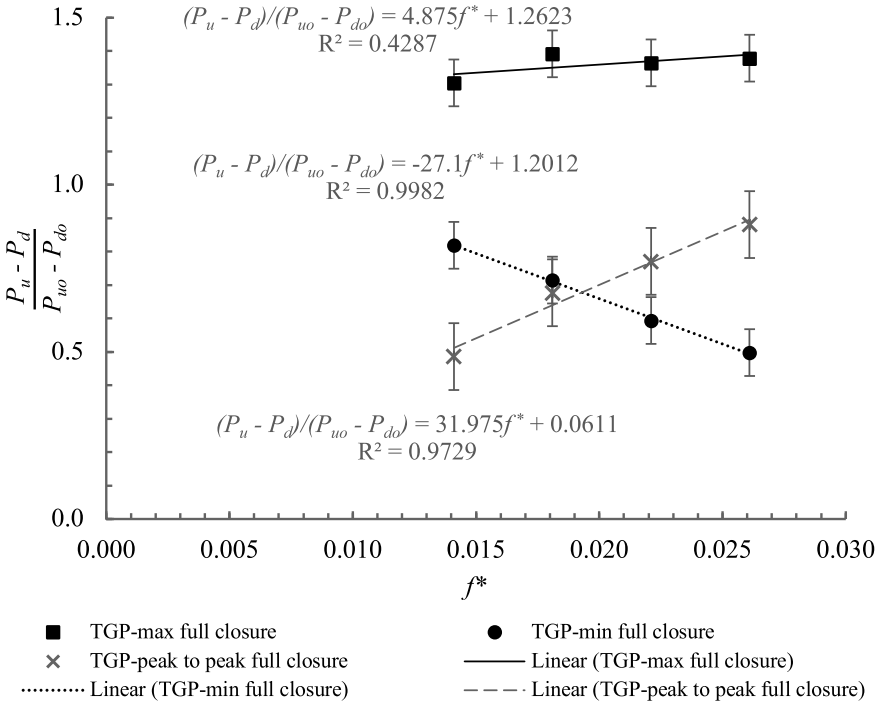

FIG. 12. Plots of the maxima, minima, and peak-to-peak differentials of the transglottal pressure time traces as a function of reduced frequency for fully closed vocal folds shown in Fig. 9(a). Linear regression fits along with the regression equations and correlation coefficients are included.

C. Frequency effects and extrapolation to higher frequencies

While there are differences between the full and incomplete closure cases, as discussed above, the challenge in this final section is to try to separate frequency effects from variations due to incomplete closure. This was done by identifying key "landmarks" in the phase-averaged momentum traces presented in Sec. IV for the fully closed cases alone, and then again for the incomplete closure cases. For simplicity, only analysis for the fully closed cases is presented here. However, the trends for the incomplete closure cases are consistent with those of the fully closed cases.

Given that the transglottal pressure force is the driver in the streamwise momentum equation, the obvious first thing to examine is its frequency dependence. This dependence does not immediately emerge from the scaling analysis in Sec. I C because the transglottal pressure force is the nondimensionalizing parameter for all other terms. To examine this dependence, maxima and minima of transglottal pressure force time traces for the fully closed cases, shown in Fig. 9(a), were plotted as a function of reduced frequency. These appear in Fig. 12. Solid squares and circles represent values for the maxima and minima, respectively. In addition, the peak-to-peak transglottal pressure difference, that is, the difference between the maxima and minima at each frequency, is plotted as $\times'$s. Linear regression fits for the three data sets have also been included. The equation for each line and the respective correlation coefficient appear to the left of the corresponding data.

Before proceeding, it is important to note that this model was scaled to the male voice. One must therefore proceed with caution in extrapolating across the entire range of human phonation. This caveat applies to the entirety of the analysis in this subsection. With that said, there is value both in looking at the frequency range covered in this study as well as contemplating what might happen at higher frequencies.

The striking feature of Fig. 12 is how transglottal pressure varies linearly with reduced frequency over the range examined. In particular, the minima decrease linearly with increasing f^* and the peak-to-peak difference also varies linearly with f^*. While the regression line for transglottal pressure maxima indicates a weak increase with reduced frequency, it is also possible that this is frequency-independent in the range of frequencies studied. Though not shown, trends for the incomplete closure cases are similar; this is consistent with the idea that frequency dependence can be decoupled from whether or not the vocal folds close completely.

It is hypothesized that the trends observed in Fig. 12 must be limited to low frequencies. It is simply nonphysical for the downstream, supraglottal pressure, P_d, to exceed the upstream, subglottal pressure. Hence the minima of the traces in Fig. 10(a) could not reach zero. Indeed, it seems implausible that the minima would even approach zero. If one were to extrapolate the regression line for the transglottal pressure minima, it would cross zero, i.e., $P_d = P_u$, when f^* reached 0.0443. This corresponds to an equivalent human frequency of 165 Hz, well within the range of human phonation. While the full meaning of this is not yet known at this point, it is clear that the linear relations seen in Fig. 12 cannot extend across all voice frequencies.

With these constraints in mind, recall that minimum transglottal pressure occurs around the time when the vocal folds are fully open. This implies that frequency dependences would be most prevalent then. At higher frequencies, the opening time of the folds is much shorter, meaning that the glottal jet must be much more impulsive and there is a greater pressure drop with increasing frequency. As will be discussed below, there appears to be a concomitant increase in the inertia term with frequency when the vocal folds are open as well. In combination, this would indicate a change in the dynamic balance with increasing frequency. This is a subject for future study.

It is a matter of curiosity that the regression line for the peak-to-peak differential comes very close to passing through the origin. Artificially adding the origin as a data point changes the slope of the regression fit to just 34.41, an increase of 7.6%, and the intercept decreases to 0.0097. The adjusted correlation coefficient increases to 0.994. The physical meaning of this is not immediately obvious. Whether the vocal folds are open or closed at zero reduced frequency, i.e., no vocal fold motion, it is nonphysical for the transglottal pressure to be zero. So again, it appears that there must be a deviation from the trend seen in Fig. 12 at lower frequencies. The key difference here is that frequencies below those studied here are well below the range of human speech and are therefore of lesser interest.

A similar analysis was conducted for the phase-averaged vocal fold drag time signatures appearing in Fig. 10(a). This too does not explicitly appear in the scaling analysis of Sec. I C. Maxima, minima, and peak-to-peak measures of vocal fold drag are shown in Fig. 13. Interestingly, here the linear dependencies on frequency are not as strong as for the transglottal pressure force.

A major factor for the difference between Figs. 12 and 13 is that the vocal fold drag calculation includes the intermediate pressure measurements at $(x–x_u)/(x_d–x_u) = 0.25$ and 0.75. These measurements were used to estimate the drag contribution on the curved portion of the vocal fold model. The fact that the frequency dependence for vocal fold drag is not as strong as for the transglottal pressure force is an indicator that transglottal pressure may not be as good a surrogate for vocal fold drag at higher frequencies. It further indicates the importance of knowing the pressure distribution along the glottis as it significantly affects the drag.

Returning now to the scaling analysis presented in Sec. I C, it can be seen in Figs. 11(c) and 11(c′) that the unsteady inertia term, while small in the current frequency range, increases in proportion to frequency. Following the methodology in analyzing the phase-averaged traces in Figs. 10(a) and 11(a), maxima, minima, and peak-to-peak differentials for the unsteady inertia traces in Fig. 11(c) are plotted in Fig. 14. The origin was included as a data point for all three quantities because at zero frequency, there would be no phase-averaged unsteadiness.

As can be seen, all three quantities are well described with second-order polynomial fits. The equation for the peak-to-peak differential is included in the plot along with the correlation coefficient. Recall that Eq. (5) of the scaling analysis indicated that the ratio of unsteady inertia to the transglottal pressure force should be proportional to $8f^*$. This indicates that the unsteady

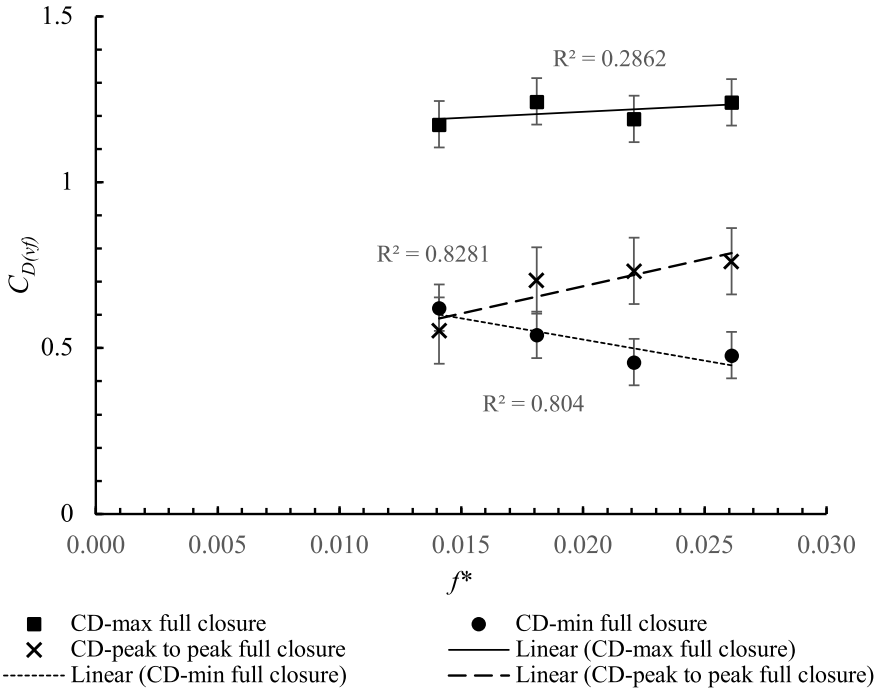

FIG. 13. Plots of the maxima, minima, and peak-to-peak differentials of the vocal fold drag time traces as a function of reduced frequency for fully closed vocal folds shown in Fig. 10(a). Linear regression fits along with the regression equations and correlation coefficients are included.

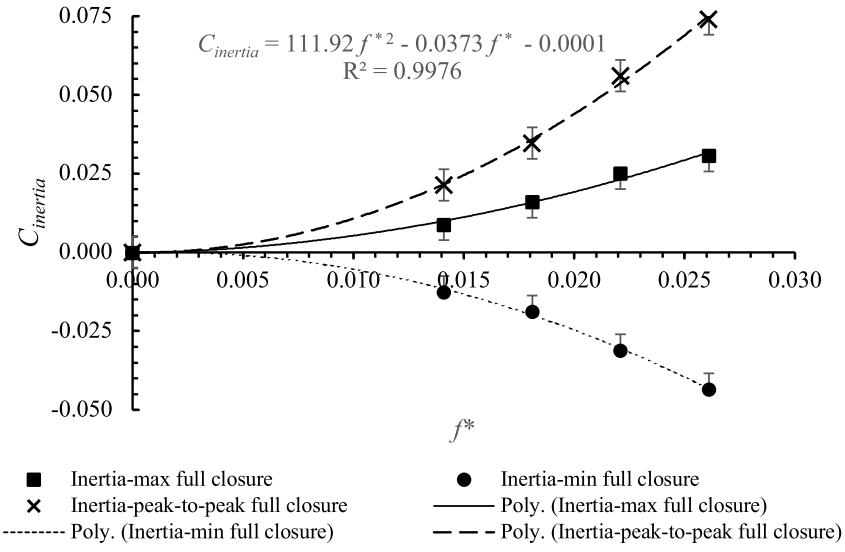

FIG. 14. Plots of the maxima, minima, and peak-to-peak differentials of time traces of the unsteady inertia term as a function of reduced frequency for fully closed vocal folds shown in Fig. 11(c). Second-order regression fits for the three parameters along with the regression equation and correlation coefficient for the peak-to-peak data are included.

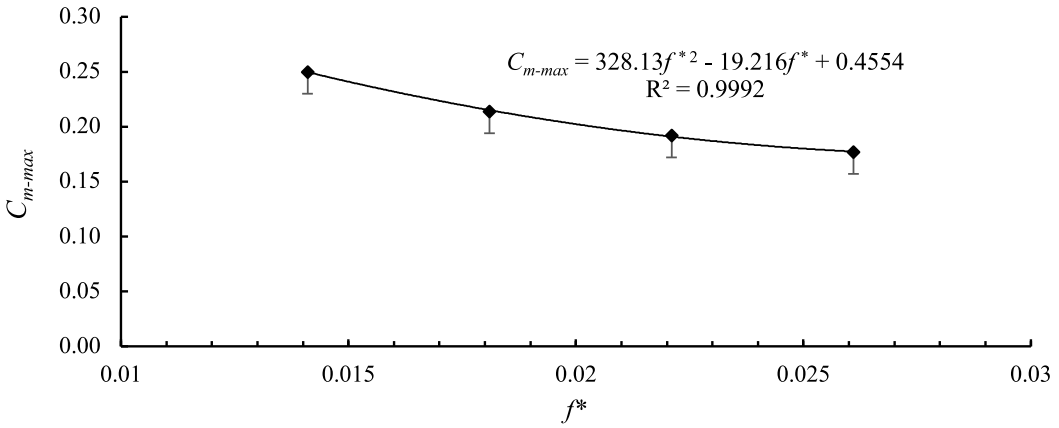

FIG. 15. Plot of the momentum flux coefficient maxima vs reduced frequency for fully closed vocal folds shown in Fig. 10(b). A second-order regression fit with the regression equation and correlation coefficient is included.

inertia term should be equal to the transglottal pressure force term around a reduced frequency of $f^* = 0.125$. For the parameters as defined in this experiment, this would correspond to a life frequency, f_{life}, of ~467 Hz. While this is higher than the typical frequency range for children and adult women, it does indicate that unsteady inertia may be significant, i.e., of the same order of magnitude, in female and child phonation, or in soprano range singing (i.e., from ~260 to ~1050 Hz). That is, the assumption of equivalence of the transglottal pressure force to vocal fold drag may not hold for higher frequencies.

The slope of the regression fit in Fig. 14 at the reduced frequency, $f^* = 0.0261$, is 5.8. This is in good agreement with the scaling analysis. An argument could be made that $T_o/2$, the amount of time when the vocal folds are open and closed, may be too long given the rapid changes that occur when the vocal folds change direction. This would imply that the coefficient in Eq. (5) would be somewhat larger and that the unsteady inertia term would become significant at proportionally lower life frequencies.

Finally, Eq. (7) indicates that the ratio of the momentum flux term to transglottal pressure force scales as $2\frac{h_{\max}}{W}$. On the one hand, this prediction is consistent with the maximum values of momentum flux in Figs. 11(b) and 11(b′). Observe that terms of the integral momentum equation in Fig. 11 were nondimensionalized by the transglottal pressure difference when the vocal folds were closed, so that Figs. 11(b) and 11(b′) represent direct comparisons to the scaling shown in Eq. (7). For this experiment, $h_{\max}$ was approximately 2.2 cm and the glottal duct width was 28 cm. So $2h_{\max}/W$ is then 0.157. By comparison, the maxima for the momentum flux terms range from ~0.1 to ~0.2.

On the other hand, however, although Eq. (7) does not predict it, frequency dependence is indeed visible in both Figs. 11(b) and 11(b′) where the general trend is a leaning of the momentum flux traces to the right and a reduction in peak amplitude with increasing frequency. This frequency dependence is further evident in the plot of maximum values of momentum flux versus reduced frequency shown in Fig. 15. If one uses a second-order polynomial fit and computes the reduced frequency at which the slope of the momentum flux versus frequency curve goes to zero, one would find that this occurs at $f^* = 0.0293$ corresponding to a life equivalent frequency of 109 Hz. If, however, using a linear fit (which has a correlation coefficient of 0.963) and extrapolating to the frequency where momentum flux becomes zero yields an intercept of $f^* = 0.0547$, this would correspond to a life frequency of 203 Hz. In either case, it appears that momentum flux reaches a minimum within the frequency range of human phonation.

Before closing, it is important to add a note on the uncertainties of these statistics. A conservative estimate for the nondimensional pressure force and vocal fold drag measurements is ± 0.07 [11]. As such, the uncertainty of the difference of the maxima and minima would be ± 0.1. These uncertainty limits are indicated in Figs. 12 and 13. The uncertainties for the maxima and minima of the unsteady inertia time traces are one-sided as the extreme values, highest and lowest, respectively, were selected. The uncertainty of the differential of the maxima and minima, however, is considered to be two-sided. Based on the largest high-frequency fluctuations in the phase-averaged unsteady inertia time traces, the one-sided uncertainties are –0.005 and +0.005 for the maxima and minima, respectively. The uncertainty of the differential is ± 0.005. These uncertainties are shown in Fig. 14. Again, the uncertainty for the maxima of the momentum flux time traces is one-sided, with the largest observed amplitude fluctuations of –0.01. This uncertainty is included in Fig. 15.

In summary, one can roughly divide incomplete closure into two categories: those that adversely affect an individual's ability to produce sound, and those that do not. Regardless of the degree of closure, however, there are clear frequency dependencies in jet speed, volume flow rate, pressure, and terms in the streamwise integral momentum equation. Further, these dependencies do not appear to be substantively different between each canonical case and its noncanonical counterpart. It is therefore reasonable to conclude that, at least to first order, it is possible to decouple incomplete closure effects from frequency effects. Based on the present data, i.e., recalling that the analysis extrapolates beyond frequency dependence trends observed in the low male frequency range, it appears that frequency effects, particularly the unsteady inertia term, may become quite significant as frequency increases from the adult male range to that of children and adult females. Though there is currently no physical explanation, the present statistical analysis coupled with the scaling analysis, specifically Eq. (5), indicates that the unsteady inertia term could become as important as the transglottal pressure force and vocal fold drag in the frequency range of human phonation.

VI. CONCLUSIONS

The effects of incomplete vocal fold closure on glottal jet dynamics and the implications on human phonation were examined using simultaneous DPIV and pressure measurements made in a $10\times$ scaled-up vocal fold model. Four model frequencies, 0.035, 0.045, 0.055, and 0.065 Hz, were examined corresponding to life frequencies of 52.5, 67.5, 82.5, and 97.5 Hz, respectively. They also spanned a reduced frequency range of $0.0141 \leqslant f^* \leqslant 0.0261$. The issues addressed were (i) whether and how incomplete closure affects phase-averaged glottal jet dynamics, (ii) the effect of incomplete closure on cycle-to-cycle variations, and (iii) whether and how frequency affects glottal jet dynamics. In light of these questions, we present specific conclusions drawn from the results presented in this study.

Conclusions regarding the effects of incomplete closure on jet dynamics that are independent of frequency are as follows:

(i) The jet acceleration when the vocal folds begin to open is very different in comparison to fully closed cases. For fully closed cases, the jet acceleration is much more impulsive, while it is more gradual when the folds do not completely close. This is because there is continuous flow through the vocal folds in the incomplete closure cases.

(ii) There is a reduction in the maximum-to-minimum differential in volume flow rate for the incomplete closure cases. This is primarily because there is continuous flow when the vocal folds do not close. There is, however, a small reduction in the maximum volume flow rate relative to the full closure cases.

(iii) With respect to cycle-to-cycle variations, there is no evidence of cycle-to-cycle variations for the incomplete closure cases. This is attributed to the continuous presence of a glottal jet, which ensures repeatable initial conditions for every successive oscillation cycle.

Finally, frequency effects were observed that were generally independent of whether or not the vocal folds closed completely. These are as follows:

(i) All terms in the integral momentum equation are attenuated when the vocal folds do not completely close. From a phonation perspective, the most important of these is the transglottal pressure force because it serves as a surrogate for vocal fold drag, i.e., the dominant aeroacoustic source. The strongest frequency dependence in transglottal pressure occurs when the vocal folds are fully open. This may be related to the increased importance of inertia with increasing frequency.

(ii) Both statistical analysis of phase-averaged time traces of terms in the integral streamwise momentum equation and dimensional scaling analysis indicate that the unsteady inertia term may be of the same order as the transglottal pressure force in the frequency range of human phonation. This is consistent with the observation of increased peak-to-peak transglottal pressure differences with increasing frequency noted above. It is further indication that the glottal jet dynamics at higher frequencies is significantly different from that at lower frequencies in the human phonation range.

(iii) There are variations in the downstream pressure difference, $P_g - P_d$, as a function of time and for different oscillation frequencies. These are believed to be an indication of higher-order unsteadiness when the vocal folds first open from a fully closed position, and of associated cycle-to-cycle variations in the fully closed cases. The variations are significantly reduced for the incomplete closure cases.

ACKNOWLEDGMENTS

Support from the National Institutes of Health Grant R01 DC005642-14, is gratefully acknowledged.

The authors report no conflict of interest.

[1] J. H. Jen, R. W. Chan, C.-H. Wu, and C.-T. Wang, Phonation threshold pressure/flow for reflecting glottal closure in unilateral vocal fold paralysis, Laryngoscope **131**, E1598 (2020).

[2] J. Rusz, J. Klempír, E. Baborová, T. Tykalová, V. Majerová, R. Čmejla, E. Ružička, and J. Roth, Objective acoustic quantification of phonatory dysfunction in Huntington's disease, PLoS One **8**, e65881 (2013).

[3] S. Sagiroglu, N. Bilal, and I. Orhan, A comparison of voice analysis results according to localization of vocal polyps in the vocal folds, Tr-ENT **29**, 72 (2019).

[4] I. R. Titze, *Principles of Voice Production* (Prentice Hall, Englewood Cliffs, NJ, 1994).

[5] Z. Zhang, Compensation strategies in voice production with glottal insufficiency, J. Voice **33**, 96 (2019).

[6] M. Södersten and P.-Å. Lindestad, Glottal closure and perceived breathiness during phonation in normally speaking subjects, J. Speech. Hearing Res. **33**, 601 (1990).

[7] M. Södersten, S. Hertegård, and B. Hammarberg, Glottal closure, transglottal airflow, and voice quality in healthy middle-aged women, J. Voice **9**, 182 (1995).

[8] A. M. Sulter, H. Schutte, and D. G. Miller, Standardized laryngeal videostroboscopic rating: Differences between untrained and trained male and female subjects, and effects of varying sound intensity, fundamental frequency and age, J. Voice **10**, 175 (1996).

[9] R. R. Patel, A. Dixon, A. M. Richmond, and K. D. Donohue, Pediatric high speed digital imaging of vocal fold vibration: A normative pilot study of glottal closure and phase closure characteristics, Int. J. Pediatr. Otorhinolaryngol. **76**, 954 (2012).

[10] M. Zañartu, G. E. Galindo, B. D. Erath, S. D. Peterson, G. R. Wodicka, and R. E. Hillman, Modeling the effects of a posterior glottal opening on vocal fold dynamics with implications for vocal hyperfunction, J. Acoust. Soc. Am. **136**, 3262 (2014).

[11] H. Ringenberg, D. Rogers, N Wei, M. Krane, and T. Wei, Phase-averaged and cycle-to-cycle analysis of jet dynamics in a scaled up vocal fold model, J. Fluid Mech. **918**, A44 (2021).

[12] M. H. Krane, M. Barry, and T. Wei, Dynamics of temporal variations in phonatory flow, J. Acoust. Soc. Am. **128**, 372 (2010).

[13] R. Mittal, B. D. Erath, and M. W. Plesniak, Fluid dynamics of human phonation and speech, Ann. Rev. Fluid Mech. **45**, 437 (2013).

[14] L. Oren, S. Khosla, and E. Gutmark, Intraglottal pressure distribution computed from empirical velocity data in canine larynx, J. Biomech. **47**, 1287 (2014).
[15] M. Dollinger, D. A. Berry, and G. S. Berke, Medial surface dynamics of an in vivo canine vocal fold during phonation, J. Acoust. Soc. Am. **117**, 3174 (2005).
[16] B. D. Erath and M. W. Plesniak, An investigation of asymmetric flow features in a scaled up driven model on the human vocal folds, Exp. Fluids **49**, 131 (2010).
[17] P. R. Murray and S. L. Thomson, Vibratory responses of synthetic, self-oscillating vocal fold models, J. Acoust. Soc. Am. **132**, 3428 (2012).
[18] J. Neubauer, Z. Zhang, R. Miraghaie, and D. A. Berry, Coherent structures of the near field flow in a self-oscillating physical model of vocal folds, J. Acoust. Soc. Am. **121**, 1102 (2007).
[19] J. S. Drechsel and S. L. Thomson, Influence of supraglottal structures on the glottal jet exiting a two-layer synthetic, self-oscillating vocal fold model, J. Acoust. Soc. Am. **123**, 4434 (2008).
[20] P. Sidlof, O. Doaré, O. Cadot, and A. Chaigne, Measurement of flow separation in a human vocal folds model, Exp. Fluids **51**, 123 (2011).
[21] F. Krebs, F. Silva, D Sciamarella, and G. Artana, A three-dimensional study of the glottal jet, Exp. Fluids **52**, 1133 (2012).
[22] A. Lodermeyer, M. Tautz, S. Becker, M. Döllinger, V. Birk, and S. Kniesburges, Aeroacoustic analysis of the human phonation process based on a hybrid acoustic PIV approach, Exp. Fluids **59**, 13 (2018).
[23] C. Farbos de Luzan, S. M. Khosla, L. Oren, A. Maddox, and E. Gutmark, Relationship between intraglottal geometry, vocal tract constriction, and glottal flow during phonation of a canine larynx, J. Acoust. Soc. Am. **144**, 1767 (2018).
[24] C. Farbos de Luzan, L. Oren, A. Maddox, E. Gutmark, and S. M. Khosla, Volume velocity in a canine larynx model using time-resolved tomographic particle image velocimetry, Exp. Fluids **61**, 63 (2020).
[25] X. Zheng, R. Mittal, Q. Xue, and S. Bielamowicz, Direct-numerical simulation of the glottal jet and vocal-fold dynamics in a three-dimensional laryngeal model, J. Acoust. Soc. Am. **130**, 404 (2011).
[26] M. Kaltenbacher, S. Zörner, A. Hüppe, and P. Sidlof, in *3D Numerical Simulations of Human Phonation. 11th World Congress on Computational Mechanics*, edited by E. Oñate, J. Oliver, and A. Huerta (CIMNE, 2014).
[27] W. Mattheus and C. Brücker, Characteristics of the pulsating jet flow through a dynamic glottal model with a lens-like constrictions, Biomed. Eng. Lett. **8**, 309 (2018).
[28] H. Sadeghi, S. Kneisburges, S. Falk, M. Kaltenbacher, A. Schützenberger, and M. Döllinger, Towards a clinically applicable computational larynx model, Appl. Sci. **9**, 2288 (2019).
[29] J. B. Park and L. Mongeau, Experimental investigation of the influence of a posterior gap on glottal flow and sound, J. Acoust. Soc. Am. **124**, 1171 (2008).
[30] Z. Zhang, Restraining mechanisms in regulating glottal closure during phonation, J. Acoust. Soc. Am. **130**, 4010 (2011).
[31] B. Schneider, W. Bigenzahn, A. End, D.-M. Denk, and W. Klepetko, External vocal fold medialization in patients with recurrent nerve paralysis following cardiothoracic surgery, Eur. J. Cardiothorac. Surg. **23**, 477 (2003).
[32] P. Birkholz, B. J. Kröger, and C. Neuschaefer-Rube, Synthesis of breathy, normal, and pressed phonation using a two-mass model with a triangular glottis, *Proceedings of the 12th Annual Conference of the International Speech Communication Association* (INTERSPEECH, 2011), pp. 2681–2684.
[33] R. A. Samlan, B. H. Story, and K. Bunton, Relation of perceived breathiness to laryngeal kinematics and acoustic measures based on computational modeling, J. Speech Lang. Hearing Sci. **56**, 1209 (2013).
[34] G. E. Galindo, S. D. Peterson, B. D. Erath, C. Castro, R. E. Hillman, and M. Zañartu, Modeling the pathophysiology of phonotraumatic vocal hyperfunction with a triangular glottal model of the vocal folds, J. Speech Lang. Hearing Res. **60**, 2452 (2017).
[35] M. J. McPhail, E. T. Campo, and M. H. Krane, Aeroacoustic source characterization in a physical model of phonation, J. Acoust. Soc. Am. **146**, 1230 (2019).
[36] E. Sherman, L. Lambert, B. White, M. H. Krane, and T. Wei, Cycle-to-cycle flow variations in a square duct with a symmetrically oscillating constriction, Fluid Dyn. Res. **52**, 015505 (2020).

[37] N. Curle, The influence of solid boundaries upon aerodynamic sound, Proc. R. Soc. London A **231**, 505 (1955).
[38] J. E. Ffowcs-Williams and D. L. Hawkings, Sound generation by turbulence and surfaces in arbitrary motion, Philos. Trans. R. Soc. London, Ser. A **264**, 321 (1969).
[39] D. G. Crighton, Basic principles of aerodynamic noise generation, Prog. Aerosp. Sci. **16**, 31 (1975).
[40] M. S. Howe, Contributions to the theory of aerodynamic sound, with application to excess jet noise and the theory of the flute, J. Fluid Mech. **71**, 625 (1975).
[41] M. S. Howe and R. S. McGowan, Sound generated by aerodynamic sources near a deformable body, with application to voiced speech, J. Fluid Mech. **592**, 367 (2007).
[42] M. S. Howe and R. S. McGowan, Production of sound by unsteady throttling of flow into a resonant cavity, with application to voiced speech, J. Fluid Mech. **672**, 428 (2011).
[43] Z. Zhang, L. Mongeau, and S. Frankel, Experimental verification of the quasisteady approximation for aerodynamic sound generation by pulsating jets in tubes, J. Acoust. Soc. Am. **112**, 1652 (2002).
[44] M. Barry, M. Krane, and T. Wei, Flow characteristics in a scaled-up glottis model, J. Acoust. Soc. Am. **115**, 2611 (2004).
[45] M. H. Krane, M. Barry, and T. Wei, Unsteady behavior of flow in a scaled-up vocal folds model, J. Acoust. Soc. Am. **122**, 3659 (2007).
[46] T. Y. Hsu, Hydrodynamic stability at the exit of a papermachine headbox, Ph.D. dissertation, Rutgers, 2000.
[47] T. Y. Hsu, L. M. Grega, R. I. Leighton, and T. Wei, Turbulent kinetic energy transport in a corner formed by a solid wall and a free surface, J. Fluid Mech. **410**, 343 (2000).
[48] B. Cranen and L. Boves, Pressure measurements during speech production using semiconductor miniature pressure transducers: Impact on models for speech production, J. Acoust. Soc. Am. **77**, 1543 (1985).
[49] F. Alipour and R. C. Scherer, Pulsatile airflow during phonation: An excised larynx model, J. Acoust. Soc. Am. **97**, 1241 (1995).
[50] F. Alipour and R. C. Scherer, Time-dependent pressure and flow behavior of a self-oscillating laryngeal model with ventricular folds, J. Voice **29**, 649 (2015).
[51] F. Alipour and R. C. Scherer, Effects of oscillation of a mechanical hemilarynx model on mean transglottal pressures and flows, J. Acoust. Soc. Am. **110**, 1562 (2001).
[52] M. Deverge, X. Pelorson, C. Vilain, P.-Y. Lagrée, F. Chentoug, J. Willems, and A. Hirschberg, Influence of collision on the flow through in-vitro rigid models of the vocal folds, J. Acoust. Soc. Am. **114**, 3354 (2003).
[53] S. Iwata, H. von Leden, and D. Williams, Air flow measurement during phonation, J. Commun. Disord. **5**, 67 (1972).
[54] E. B. Holmberg, R. E. Hillman, and J. S. Perkell, Glottal airflow and transglottal air pressure measurements for male and female speakers in soft, normal, and loud voice, J. Acoust. Soc. Am. **84**, 511 (1988).
[55] E. B. Holmberg, R. E. Hillman, and J. S. Perkell, Glottal airflow and transglottal air pressure measurements for male and female speakers in low, normal, and high pitch, J. Voice **3**, 294 (1989).
[56] E. B. Holmberg, P. Doyle, J. S. Perkell, B. Hammarberg, and R. E. Hillman, Aerodynamic and acoustic voice measurements of patients with vocal nodules: Variation in baseline and changes across voice therapy, J. Voice **17**, 269 (2003).